Ceramics-Silikáty 63 (2), 131-148 (2019)
www.ceramics-silikaty.cz doi: 10.13168/cs.2019.0005

TIME-DEPENDENT MATRIX MULTI-FRACTURE OF SiC/SiC CERAMIC-MATRIX COMPOSITES CONSIDERING INTERFACE OXIDATION

LI LONGBIAO

College of Civil Aviation, Nanjing University of Aeronautics and Astronautics
No.29 Yudao St., Nanjing 210016, PR China

E-mail: llb451@nuaa.edu.cn

Submitted October 4, 2018; accepted January 7, 2019

Keywords: Ceramic-matrix composites (CMCs), Matrix multi-cracking, Time-dependent, Interface oxidation

In this paper, the time-dependent matrix multi-cracking of SiC/SiC ceramic-matrix composites (CMCs) has been investigated considering the fibre/matrix interface oxidation. The time-dependent interface oxidation length and temperature-dependent fibre/matrix interface shear stress in the oxidation and the de-bonded region, the interface de-bonded energy, the fibre and matrix modulus and the matrix fracture energy are considered in the analysis for the micro stress field, the interface debonding criterion and the critical matrix strain energy model. The effects of the fibre volume fraction, the fibre/matrix interface shear stress, the fibre/matrix interface frictional coefficient, the fibre/matrix interface de-bonded energy and the matrix fracture energy on the matrix multi-cracking density and the interface oxidation ratio of SiC/SiC composite are discussed for the different temperatures and oxidation time. The experimental matrix multi-cracking density and fibre/matrix interface oxidation ratio are predicted for unidirectional and mini SiC/SiC composites at different testing temperatures and oxidation time.

INTRODUCTION

Ceramic materials possess high specific strength and a specific modulus at elevated temperatures. But their use as structural components is severely limited due to their brittleness. Continuous fibre-reinforced ceramic-matrix composites (CMCs), by incorporating fibres in the ceramic matrices, not only exploit their attractive high-temperature strength, but also reduce the propensity for catastrophic failure [1, 2, 3]. The environment inside the hot section CMC components is harsh and the composite is typically subjected to complex thermomechanical loading, which can lead to matrix multi-cracking [4, 5]. These matrix cracks form paths for the ingress of the environment oxidising the fibres and leading to a premature failure [6, 7, 8, 9, 10]. The density and openings of these cracks depend on the fibre architecture, the fibre/matrix interface bonding intensity, the applied load and the environments [11, 12, 13]. It is important to develop an understanding of the matrix multi-cracking damage mechanisms at elevated temperatures considering the oxidation damage mechanisms. [14]

Many researchers performed experimental and theoretical investigations on the matrix multi-cracking evolution of fibre-reinforced CMCs [15, 16, 17, 18, 19, 20, 21]. Morscher et al. [22] established the relationships for the stress-dependent matrix cracking of a 2D SiC/SiC composite, which was related to the stress in the load-bearing SiC matrix. Morscher and Gordon [23] monitored the matrix cracking of a SiC/SiC matrix composite using acoustic emission (AE) and electrical resistance (ER). Racle et al. [24] established the relationship between the characteristic time of a 25 % total fatigue lifetime and the beginning of the matrix cracking using AE. However, in the studies mentioned above, the time-dependent matrix multi-cracking of the SiC/SiC composite at an elevated temperature considering the interface oxidation has not been investigated.

In this paper, the time-dependent matrix multi-cracking of a SiC/SiC composite has been investigated considering the fibre/matrix interface oxidation. The time-dependent interface oxidation length and temperature-dependent fibre/matrix interface shear stress in the oxidation and de-bonded region, the interface de-bonded energy, the fibre and matrix modulus and matrix fracture energy are considered in the analysis for the micro stress field, the interface debonding criterion and the critical matrix strain energy model. The effects of the fibre volume fraction, the fibre/matrix interface shear

stress, the fibre/matrix interface frictional coefficient, the fibre/matrix interface de-bonded energy and the matrix fracture energy on the matrix multi-cracking density and the fibre/matrix interface oxidation ratio of the SiC/SiC composite are discussed for the different temperatures and oxidation time. The experimental matrix multi-cracking density and the fibre/matrix interface oxidation ratio for the unidirectional and mini SiC/SiC composites at different testing temperatures and oxidation time are predicted.

THEORETICAL ANALYSIS

Time-dependent stress analysis

The composite with the fibre volume fraction of V_f is loaded by a remote uniform stress σ normal to the crack plane, as shown in Figure 1. The fibre radius is r_f, and the matrix radius is R ($R = r_f/V_f^{1/2}$). The length of the unit cell is half a matrix crack spacing $l_c/2$, and the interface oxidation length and interface de-bonded length are ζ and l_d, respectively. The time-dependent fibre and matrix axial stress and the fibre/matrix interface shear stress distributions can be determined using the following equations:

$$\sigma_f(z,t,T)=\begin{cases}\dfrac{\sigma}{V_f}-\dfrac{2\tau_f(T)}{r_f}z, z\in\left[0,\ \zeta(T)\right]\\ \dfrac{\sigma}{V_f}-\dfrac{2\tau_f(T)}{r_f}\zeta(t,T)-\dfrac{2\tau_i(T)}{r_f}\left[z-\zeta(t,T)\right], z\in\left[\zeta(t,T), l_d(t,T)\right]\\ \sigma_{fo}+\left[\dfrac{V_m}{V_f}\sigma_{mo}-\dfrac{2\tau_f(T)}{r_f}\zeta(t,T)-\dfrac{2\tau_i(T)}{r_f}\left[l_d(t,T)-\zeta(t,T)\right]\right]\\ \times\exp\left[-\rho\dfrac{z-l_d(t,T)}{r_f}\right], z\in\left[l_d(t,T),\dfrac{l_c(t,T)}{2}\right]\end{cases} \tag{1}$$

$$\sigma_m(z,t,T)=\begin{cases}2\dfrac{V_f}{V_m}\dfrac{\tau_f(T)}{r_f}z, z\in\left[0,\zeta(t,T)\right]\\ 2\dfrac{V_f}{V_m}\dfrac{\tau_f(T)}{r_f}\zeta(t,T)+2\dfrac{V_f}{V_m}\dfrac{\tau_i(T)}{r_f}\left[z-\zeta(t,T)\right], z\in\left[\zeta(t,T), l_d(t,T)\right]\\ \sigma_{mo}+\left[2\dfrac{V_f}{V_m}\dfrac{\tau_f(T)}{r_f}\zeta(t,T)+2\dfrac{V_f}{V_m}\dfrac{\tau_i(T)}{r_f}\left[l_d(t,T)-\zeta(t,T)\right]-\sigma_{mo}\right]\\ \times\exp\left[-\rho\dfrac{z-l_d(t,T)}{r_f}\right], z\in\left[l_d(t,T),\dfrac{l_c(t,T)}{2}\right]\end{cases} \tag{2}$$

$$\tau_i(z,t,T)=\begin{cases}\tau_f(T), z\in\left[0,\zeta(t,T)\right]\\ \tau_i(T), z\in\left[\zeta(t,T), l_d(t,T)\right]\\ \dfrac{\rho}{2}\left[\dfrac{V_m}{V_f}\sigma_{mo}-\dfrac{2\tau_f(T)}{r_f}\zeta(t,T)-\dfrac{2\tau_i(T)}{r_f}\left[l_d(t,T)-\zeta(t,T)\right]\right]\\ \times\exp\left[-\rho\dfrac{z-l_d(t,T)}{r_f}\right], z\in\left[l_d(t,T),\dfrac{l_c(t,T)}{2}\right]\end{cases} \tag{3}$$

where

$$\zeta(t,T)=\varphi_1(T)\left[1-\exp\left(-\frac{\varphi_2(T)t}{b}\right)\right] \tag{4}$$

$$\tau_i(T)=\tau_0+\mu\frac{|\alpha_{rf}(T)-\alpha_{rm}(T)|(T_m-T)}{A} \tag{5}$$

$$\tau_f(T)=\tau_s+\mu\frac{|\alpha_{rf}(T)-\alpha_{rm}(T)|(T_m-T)}{A} \tag{6}$$

$$\sigma_{fo}=\frac{E_f(T)}{E_c(T)}\sigma+E_f(T)(\alpha_{lc}-\alpha_{lf})\,\Delta T \tag{7}$$

$$\sigma_{mo}=\frac{E_m(T)}{E_c(T)}\sigma+E_m(T)(\alpha_{lc}-\alpha_{lm})\,\Delta T \tag{8}$$

where $E_f(T)$, $E_m(T)$ and $E_c(T)$ denote the temperature-dependent fibre, matrix and composite elastic modulus, respectively; α_{rf} and α_{rm} denote the fibre and matrix radial thermal expansion coefficient, respectively; α_{lf}, α_{lm} and α_{lc} denote the fibre, matrix and composite axial thermal expansion coefficient, respectively; and ΔT denotes the temperature difference between the fabricated temperature T_0 and the testing temperature T_1 ($\Delta T = T_1 - T_0$).

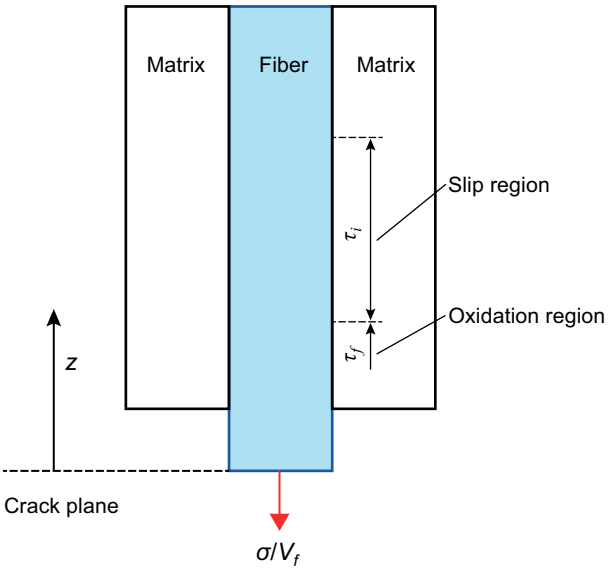

Figure 1. The schematic of the shear-lag model considering the interface oxidation and debonding.

Time-dependent fibre/matrix interface debonding

The fracture mechanics approach is adopted in the present analysis to determine the fibre/matrix interface de-bonded length. [25]

$$\gamma_d(T) = \frac{F}{4\pi r_f}\frac{\partial w_f(z=0)}{\partial l_d}\frac{1}{2} - \int_0^{l_d(t,T)} \tau_i(T)\frac{\partial v(z)}{\partial l_d}dz \quad (9)$$

where $F(=\pi r_f^2/V_f)$ denotes the fibre load at the matrix cracking plane; $w_f(z=0)$ denotes the fibre axial displacement at the matrix cracking plane and $v(z)$ denotes the relative displacement between the fibre and the matrix. Based on the fibre and matrix axial stress distribution as described in Equations 1 and 2, the fibre and matrix axial displacements of $w_f(z)$ and $w_m(z)$ can be described using the following equations:

$$\begin{aligned} w_f(z) &= \int_z^{\frac{l_c(t,T)}{2}} \frac{\sigma_f(z,t,T)}{E_f(T)}dz \\ &= \frac{\sigma}{V_f E_f(T)}\left[l_d(t,T)-z\right] - \frac{\tau_f(T)}{r_f E_f(T)}\left[2\zeta(t,T)l_d(t,T)-\zeta^2(t,T)-z^2\right] \\ &\quad - \frac{\tau_i(T)}{r_f E_f(T)}\left[l_d(t,T)-\zeta(t,T)\right]^2 + \frac{\sigma_{fo}(T)}{E_f(T)}\left[\frac{l_c(t,T)}{2}-l_d(t,T)\right] \\ &\quad + \frac{r_f}{\rho E_f(T)}\left\{\frac{V_m}{V_f}\sigma_{mo}(T) - \frac{2\tau_f(T)}{r_f}\zeta(t,T) - \frac{2\tau_i(T)}{r_f}\left[l_d(t,T)-\zeta(t,T)\right]\right\} \\ &\quad \times\left\{1-\exp\left[-\rho\frac{l_c(t,T)/2-l_d(t,T)}{r_f}\right]\right\} \end{aligned} \quad (10)$$

$$\begin{aligned} w_m(z) &= \int_z^{\frac{l_c(t,T)}{2}} \frac{\sigma_m(z,t,T)}{E_m(T)}dz \\ &= \frac{V_f\tau_f(T)}{r_f V_m E_m(T)}\left[2\zeta(t,T)l_d(t,T)-\zeta^2(t,T)-z^2\right] \\ &\quad + \frac{V_f\tau_i(T)}{r_f V_m E_m(T)}\left[l_d(t,T)-\zeta(t,T)\right]^2 + \frac{\sigma_{mo}(T)}{E_m(T)}\left[\frac{l_c(t,T)}{2}-l_d(t,T)\right] \\ &\quad - \frac{r_f}{\rho E_m(T)}\left\{\sigma_{mo}(T) - 2\frac{V_f\tau_f(T)}{r_f V_m}\zeta(t,T) - 2\frac{V_f\tau_i(T)}{r_f V_m}\left[l_d(t,T)-\zeta(t,T)\right]\right\} \\ &\quad \times\left\{1-\exp\left[-\rho\frac{l_c(t,T)/2-l_d(t,T)}{r_f}\right]\right\} \end{aligned} \quad (11)$$

The relative displacement of $v(z)$ between the fibre and the matrix can be described using the following equation:

$$\begin{aligned} v(z) &= |w_{\mathrm{f}}(z) - w_{\mathrm{m}}(z)| \\ &= \frac{\sigma}{V_{\mathrm{f}}E_{\mathrm{f}}(T)}\left[l_{\mathrm{d}}(t,T)-z\right]-\frac{E_{\mathrm{c}}(T)\tau_{\mathrm{f}}(T)}{r_{\mathrm{f}}V_{\mathrm{m}}E_{\mathrm{m}}(T)E_{\mathrm{f}}(T)}\left[2\zeta(t,T)l_{\mathrm{d}}(t,T)-\zeta^2(t,T)-z^2\right] \\ &-\frac{E_{\mathrm{c}}(T)\tau_{\mathrm{i}}(T)}{r_{\mathrm{f}}V_{\mathrm{m}}E_{\mathrm{m}}(T)E_{\mathrm{f}}(T)}\left[l_{\mathrm{d}}(t,T)-\zeta(t,T)\right]^2 \\ &+\frac{r_{\mathrm{f}}E_{\mathrm{c}}(T)}{\rho V_{\mathrm{m}}E_{\mathrm{m}}(T)E_{\mathrm{f}}(T)}\left\{\sigma_{\mathrm{mo}}(T)-2\frac{\tau_{\mathrm{f}}(T)}{r_{\mathrm{f}}}\zeta(t,T)-2\frac{\tau_{\mathrm{i}}(T)}{r_{\mathrm{f}}}\left[l_{\mathrm{d}}(t,T)-\zeta(t,T)\right]\right\} \\ &\times\left\{1-\exp\left[-\rho\frac{l_{\mathrm{c}}(t,T)/2-l_{\mathrm{d}}(t,T)}{r_{\mathrm{f}}}\right]\right\} \end{aligned} \tag{12}$$

Substituting $w_{\mathrm{f}}(z = 0)$ and $v(z)$ into Equation 9, leads to the following equation:

$$\begin{aligned} &\frac{E_{\mathrm{c}}(T)\tau_{\mathrm{i}}^2(T)}{r_{\mathrm{f}}V_{\mathrm{m}}E_{\mathrm{m}}(T)E_{\mathrm{f}}(T)}\left[l_{\mathrm{d}}(t,T)-\zeta(t,T)\right]^2+\frac{E_{\mathrm{c}}(T)\tau_{\mathrm{i}}^2(T)}{\rho V_{\mathrm{m}}E_{\mathrm{m}}(T)E_{\mathrm{f}}(T)}\left[l_{\mathrm{d}}(t,T)-\zeta(t,T)\right] \\ &-\frac{\tau_{\mathrm{i}}(T)\sigma}{V_{\mathrm{f}}E_{\mathrm{f}}(T)}\left[l_{\mathrm{d}}(t,T)-\zeta(t,T)\right]+\frac{2E_{\mathrm{c}}(T)\tau_{\mathrm{f}}(T)\tau_{\mathrm{i}}(T)}{r_{\mathrm{f}}V_{\mathrm{m}}E_{\mathrm{m}}(T)E_{\mathrm{f}}(T)}\zeta(t,T)\left[l_{\mathrm{d}}(t,T)-\zeta(t,T)\right] \\ &-\frac{r_{\mathrm{f}}\tau_{\mathrm{i}}(T)\sigma}{2\rho V_{\mathrm{f}}E_{\mathrm{f}}(T)}+\frac{E_{\mathrm{c}}(T)\tau_{\mathrm{f}}^2(T)}{r_{\mathrm{f}}V_{\mathrm{m}}E_{\mathrm{m}}(T)E_{\mathrm{f}}(T)}\zeta^2(t,T)+\frac{E_{\mathrm{c}}(T)\tau_{\mathrm{f}}(T)\tau_{\mathrm{i}}(T)}{\rho V_{\mathrm{m}}E_{\mathrm{m}}(T)E_{\mathrm{f}}(T)}\zeta(t,T) \\ &-\frac{\tau_{\mathrm{f}}(T)\sigma}{V_{\mathrm{f}}E_{\mathrm{f}}(T)}\zeta(t,T)+\frac{r_{\mathrm{f}}V_{\mathrm{m}}E_{\mathrm{m}}(T)\sigma^2}{4V_{\mathrm{f}}^2E_{\mathrm{f}}(T)E_{\mathrm{c}}(T)}-\gamma_{\mathrm{d}}(T)=0 \end{aligned} \tag{13}$$

Solving Equation 13, the fibre/matrix interface de-bonded length can be determined by the following equation:

$$l_{\mathrm{d}}(t,T)=\left[1-\frac{\tau_{\mathrm{f}}(T)}{\tau_{\mathrm{i}}(T)}\right]\zeta(t,T)+\frac{r_{\mathrm{f}}}{2}\left[\frac{V_{\mathrm{m}}E_{\mathrm{m}}(T)\sigma}{V_{\mathrm{f}}E_{\mathrm{c}}(T)\tau_{\mathrm{i}}(T)}-\frac{1}{\rho}\right]-\sqrt{\left(\frac{r_{\mathrm{f}}}{2\rho}\right)^2+\frac{r_{\mathrm{f}}V_{\mathrm{m}}E_{\mathrm{m}}(T)E_{\mathrm{f}}(T)}{E_{\mathrm{c}}(T)\tau_{\mathrm{i}}^2(T)}\gamma_{\mathrm{d}}(T)} \tag{14}$$

Time-dependent matrix multi-fracture

The temperature-dependent matrix strain energy can be described using the following equation: [26]

$$U_{\mathrm{m}}(t,T)=\frac{1}{2E_{\mathrm{m}}(T)}\int_{A_{\mathrm{m}}}\int_0^{l_{\mathrm{c}}(T)}\sigma_{\mathrm{m}}^2(z,t,T)\,dz dA_{\mathrm{m}} \tag{15}$$

where A_{m} is the cross-section area of the matrix in the unit cell.

When the interface is partially de-bonded, substituting the matrix axial stress in Equation 2 into Equation 15, the matrix strain energy can be described using the following equation:

$$\begin{aligned} U_{\mathrm{m}}(t,T) &= \frac{A_{\mathrm{m}}}{E_{\mathrm{m}}}\left\{\frac{4}{3}\left(\frac{V_{\mathrm{f}}}{V_{\mathrm{m}}}\frac{\tau_{\mathrm{f}}(T)}{r_{\mathrm{f}}(T)}\right)^2\zeta^3(t,T)+4\left(\frac{V_{\mathrm{f}}}{V_{\mathrm{m}}}\frac{\tau_{\mathrm{f}}(T)}{r_{\mathrm{f}}}\right)^2\left[l_{\mathrm{d}}(t,T)-\zeta(t,T)\right]\zeta^2(t,T)\right. \\ &+4\left(\frac{V_{\mathrm{f}}}{r_{\mathrm{f}}V_{\mathrm{m}}}\right)^2\tau_{\mathrm{f}}(T)\tau_{\mathrm{i}}(T)\zeta(t,T)\left[l_{\mathrm{d}}(t,T)-\zeta(t,T)\right]^2 \\ &+\frac{4}{3}\left[\frac{V_{\mathrm{f}}}{V_{\mathrm{m}}}\frac{\tau_{\mathrm{i}}(T)}{r_{\mathrm{f}}}\right]^2\left[l_{\mathrm{d}}(t,T)-\zeta(t,T)\right]^3+\sigma_{\mathrm{mo}}^2\left[\frac{l_{\mathrm{c}}(t,T)}{2}-l_{\mathrm{d}}(t,T)\right] \\ &+\frac{2r_{\mathrm{f}}\sigma_{\mathrm{mo}}(T)}{\rho}\left[2\frac{V_{\mathrm{f}}}{V_{\mathrm{m}}}\frac{\tau_{\mathrm{f}}(T)}{r_{\mathrm{f}}}\zeta(t,T)+2\frac{V_{\mathrm{f}}}{V_{\mathrm{m}}}\frac{\tau_{\mathrm{i}}(T)}{r_{\mathrm{f}}}\left[l_{\mathrm{d}}(t,T)-\zeta(t,T)\right]-\sigma_{\mathrm{mo}}(T)\right] \\ &\times\left[1-\exp\left(-\rho\frac{l_{\mathrm{c}}(t,T)/2-l_{\mathrm{d}}(t,T)}{r_{\mathrm{f}}}\right)\right]+\frac{r_{\mathrm{f}}}{2\rho}\left[2\frac{V_{\mathrm{f}}}{V_{\mathrm{m}}}\frac{\tau_{\mathrm{f}}(T)}{r_{\mathrm{f}}}\zeta(t,T)+2\frac{V_{\mathrm{f}}}{V_{\mathrm{m}}}\frac{\tau_{\mathrm{i}}(T)}{r_{\mathrm{f}}}\left(l_{\mathrm{d}}(t,T)-\zeta(t,T)\right)-\sigma_{\mathrm{mo}}(T)\right]^2 \\ &\left.\times\left[1-\exp\left(-2\rho\frac{l_{\mathrm{c}}(t,T)/2-l_{\mathrm{d}}(t,T)}{r_{\mathrm{f}}}\right)\right]\right\} \end{aligned} \tag{16}$$

When the interface is completely de-bonded, the matrix strain energy can be described using the following equation:

$$U_{\mathrm{m}}(t,T)=\frac{A_{\mathrm{m}}}{E_{\mathrm{m}}}\left\{\frac{4}{3}\left[\frac{V_{\mathrm{f}}}{V_{\mathrm{m}}}\frac{\tau_{\mathrm{f}}(T)}{r_{\mathrm{f}}}\right]^2\zeta^3(t,T)+4\left[\frac{V_{\mathrm{f}}}{V_{\mathrm{m}}}\frac{\tau_{\mathrm{f}}(T)}{r_{\mathrm{f}}}\right]^2\right.$$
$$\left[l_{\mathrm{d}}(t,T)-\zeta(t,T)\right]\zeta^2(t,T)+4\left(\frac{V_{\mathrm{f}}}{r_{\mathrm{f}}V_{\mathrm{m}}}\right)^2 \quad (17)$$
$$\tau_{\mathrm{f}}(T)\tau_{\mathrm{i}}(T)\zeta(t,T)\left[l_{\mathrm{d}}(t,T)-\zeta(t,T)\right]^2$$
$$\left.+\frac{4}{3}\left[\frac{V_{\mathrm{f}}}{V_{\mathrm{m}}}\frac{\tau_{\mathrm{i}}(T)}{r_{\mathrm{f}}}\right]^2\left[l_{\mathrm{d}}(t,T)-\zeta(t,T)\right]^3\right\}$$

The critical matrix strain energy of U_{mcr} can be described using the following equation:

$$U_{\mathrm{mcr}}(T)=\frac{1}{2}kA_{\mathrm{m}}l_0\frac{\sigma^2_{\mathrm{mocr}}(T)}{E_{\mathrm{m}}(T)} \quad (18)$$

where K ($k \in [0,1]$) is the critical matrix strain energy parameter; l_0 is the initial matrix crack spacing; and $\sigma_{\mathrm{mocr}}(T)$ can be described using the following equation:

$$\sigma_{\mathrm{mocr}}(T)=\frac{E_{\mathrm{m}}(T)}{E_{\mathrm{c}}(T)}\sigma_{\mathrm{cr}}(T)+E_{\mathrm{m}}(T)\left[\alpha_{\mathrm{lc}}(T)-\alpha_{\mathrm{lm}}(T)\right]\Delta T \quad (19)$$

where $\sigma_{\mathrm{cr}}(T)$ denotes the temperature-dependent critical stress corresponding to the composite's proportional limit stress defined by the ACK model: [15]

$$\sigma_{\mathrm{cr}}(T)=\left[\frac{6V_{\mathrm{f}}^2E_{\mathrm{f}}(T)E_{\mathrm{c}}^2(T)\tau_{\mathrm{i}}(T)\gamma_{\mathrm{m}}(T)}{r_{\mathrm{f}}V_{\mathrm{m}}E_{\mathrm{m}}^2(T)}\right]^{1/3}- \quad (20)$$
$$-E_{\mathrm{c}}(T)\left[\alpha_{\mathrm{lc}}(T)-\alpha_{\mathrm{lm}}(T)\right]\Delta\mathrm{T}$$

where $\gamma_{\mathrm{m}}(T)$ denotes the temperature-dependent matrix fracture energy.

The matrix multi-cracking evolution can be determined using the following equation:

$$U_{\mathrm{m}}(\sigma,t,T)=U_{\mathrm{crm}}(\sigma_{\mathrm{cr}},T) \quad (21)$$

RESULTS AND DISCUSSIONS

The ceramic composite system of SiC/SiC is used for the case study and its material properties are given by: V_{f} = 30 %, r_{f} = 7.5 μm, E_{f} = 230 GPa, γ_{m} = 15 J·m^{-2}, γ_{d} = 0.4 J·m^{-2}, τ_0 = 10 MPa, $\alpha_{\mathrm{rf}} = 2.9 \times 10^{-6}$ K^{-1} and $\alpha_{\mathrm{lf}} = 3.9 \times 10^{-6}$ K^{-1}.

The temperature-dependent SiC matrix elastic modulus of $E_{\mathrm{m}}(T)$ can be described using the following equation: [27]

$$E_{\mathrm{m}}(T)=\frac{350}{460}\left[460-0.04T\exp\left(-\frac{962}{T}\right)\right],\ T\in[300\text{-}1773\ \mathrm{K}] \quad (22)$$

The temperature-dependent SiC matrix axial and radial thermal expansion coefficients of $\alpha_{\mathrm{lm}}(T)$ and $\alpha_{\mathrm{rm}}(T)$ can be described using the following equation, respectively: [27]

$$\alpha_{\mathrm{lm}}(T)=\alpha_{\mathrm{rm}}(T)=\begin{cases}-1.8276+0.0178T-1.5544\cdot10^{-5}T^2\\ +4.5246\cdot10^{-9}T^3,\ T\in[125\text{-}1273\ \mathrm{K}]\\ 5.0\cdot10^{-6}/\mathrm{K},\ T>1273\ \mathrm{K}\end{cases} \quad (23)$$

The temperature dependent fibre/matrix interface de-bonded energy of $\zeta_{\mathrm{d}}(T)$ and the matrix fracture energy of $\zeta_{\mathrm{m}}(T)$ can be described using the following equations, respectively: [28]

$$\gamma_{\mathrm{d}}(T)=\gamma_{\mathrm{d}}^{\mathrm{o}}\left[1-\frac{\int_{T_{\mathrm{o}}}^{T}C_P(T)\,dT}{\int_{T_{\mathrm{o}}}^{T_{\mathrm{m}}}C_P(T)\,dT}\right] \quad (24)$$

$$\gamma_{\mathrm{m}}(T)=\gamma_{\mathrm{m}}^{\mathrm{o}}\left[1-\frac{\int_{T_{\mathrm{o}}}^{T}C_P(T)\,dT}{\int_{T_{\mathrm{o}}}^{T_{\mathrm{m}}}C_P(T)\,dT}\right] \quad (25)$$

where T_{o} denotes the reference temperature; T_{m} denotes the fabricated temperature; $\gamma_{\mathrm{d}}^{\mathrm{o}}$ and $\gamma_{\mathrm{m}}^{\mathrm{o}}$ denote the fibre/matrix interface de-bonded energy and the matrix fracture energy at the reference temperature of T_{o}; and $\mathrm{C_P}(T)$ can be described using the following equation:

$$C_P(T)=76.337+109.039\times10^{-3}T- \quad (26)$$
$$-6.535\times10^{5}T^{-2}-6.535\times10^{-6}T^{2}$$

The effects of the fibre volume fraction, the fibre/matrix interface shear stress, the fibre/matrix interface frictional coefficient, the fibre/matrix interface de-bonded energy and the matrix fracture energy on the time-dependent matrix multi-cracking density and the interface oxidation ratio are discussed.

Effect of the fibre volume fraction

The effect of the fibre volume fraction (i.e., V_{f} = 25 %, 30 % and 35 %) on the time-dependent matrix multi-cracking and the fibre/matrix interface oxidation ratio of the SiC/SiC composite at T = 873 K, 973 K and 1073 K for the oxidation time of t = 1 h and 3 h are shown in Figure 2.

When V_{f} = 25 % at T = 873 K and t = 1 h, the matrix multi-cracking density increases from φ = 1.2/mm at σ_{cr} = = 110 MPa to φ = 11.9/mm at σ_{sat} = 120 MPa, and the fibre/matrix interface oxidation ratio decreases from ζ/l_{d} = 6 % to ζ/l_{d} = 3.4 %; and at t = 3 h, the matrix multi-cracking density increases from φ = 0.67 mm at σ_{cr} = 110 MPa to φ = 10.7/mm at σ_{sat} =123 MPa, and the interface oxidation ratio decreases from ζ/l_{d} = 16.6 % to ζ/l_{d} = 9.8 %. At T = 973 K and t = 1 h, the matrix multi-cracking density increases from φ = 0.24/mm at σ_{cr} = 104 MPa to φ = = 9.2/mm at σ_{sat} = 133 MPa, and the interface oxidation ratio decreases from ζ/l_{d} = 16.7 % to ζ/l_{d} = 9.5 %; and at

t = 3 h, the matrix multi-cracking density increases from φ = 0.17/mm at σ_{cr} = 104 MPa to φ = 7.4/mm at σ_{sat} = = 140 MPa, and the interface oxidation ratio decreases from ζ/l_d = 40.5 % to ζ/l_d = 25.1 %. At T = 1073 K and t = 1 h, the matrix multi-cracking density increases from φ = 0.15/mm at σ_{cr} = 96 MPa to φ = 7/mm at σ_{sat} = 144 MPa, and the interface oxidation ratio decreases from ζ/l_d = = 6.7 % to ζ/l_d = 21.1 %; and at t = 3 h, the matrix multi-

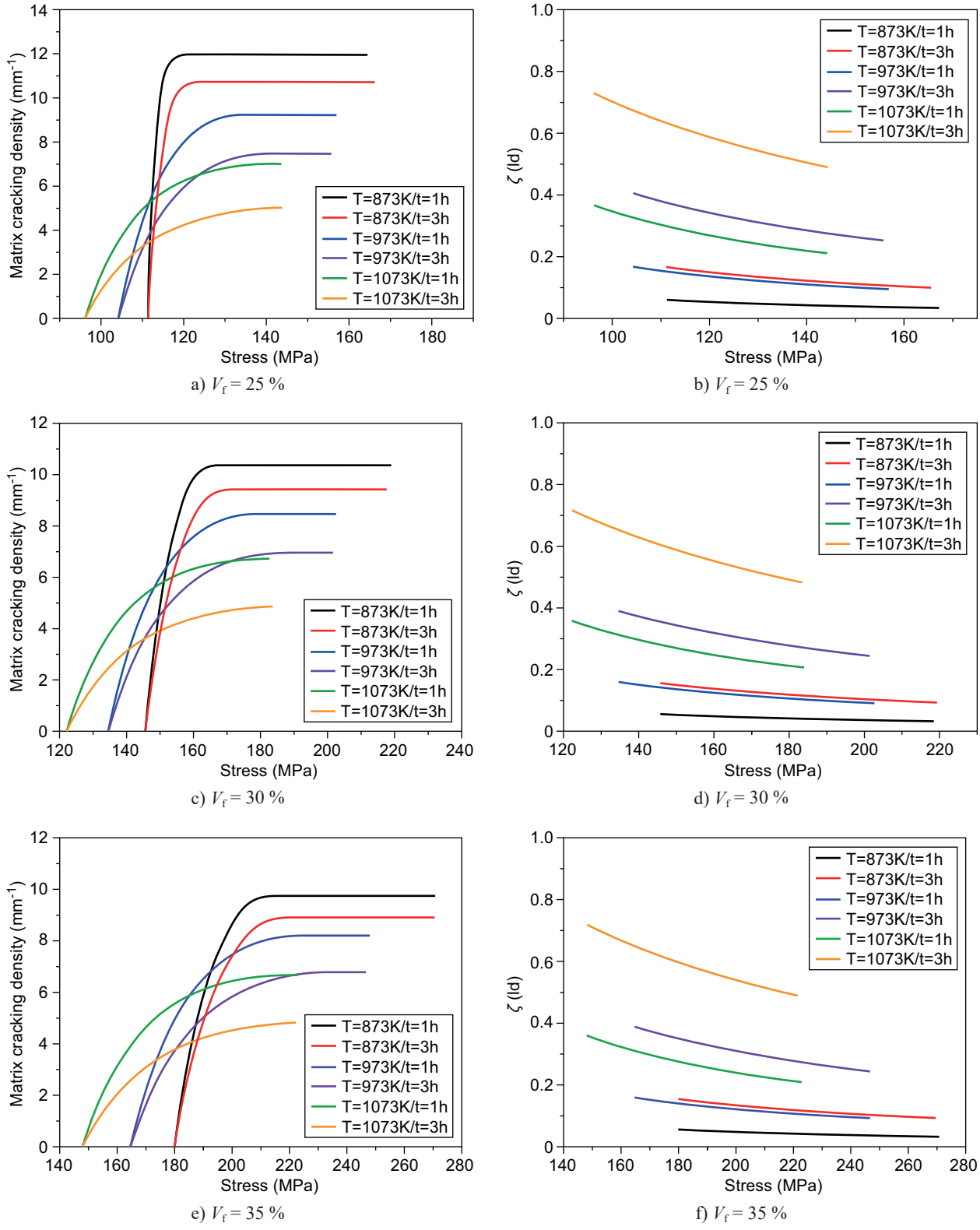

a) V_f = 25 % b) V_f = 25 %

c) V_f = 30 % d) V_f = 30 %

e) V_f = 35 % f) V_f = 35 %

Figure 2. The matrix cracking density versus the applied stress curves for the different oxidation temperature and time when V_f = 25 % (a), 30 % (c), 35 % (e); the interface oxidation ratio versus the applied stress curves for the different oxidation temperature and time when V_f = 25 % (b), 30 % (d), 35 % (f).

cracking density increases from φ = 0.09/mm at σ_{cr} = = 96.3 MPa to φ = 5.0/mm at σ_{sat} = 144 MPa, and the interface oxidation ratio decreases from ζ/l_d = 72.8 % to ζ/l_d = 48.9 %.

When V_f = 30 % at T = 873 K and t = 1 h, the matrix multi-cracking density increases from φ = 0.47/mm at σ_{cr} = 146 MPa to φ = 10.36/mm at σ_{sat} = 167 MPa, and the fibre/matrix interface oxidation ratio decreases from ζ/l_d = 5.6 % to ζ/l_d = 3.2 %; and at t = 3 h, the matrix multi-cracking density increases from φ = 0.35/mm at σ_{cr} = 146 MPa to φ = 3.4/mm at σ_{sat} = 170 MPa, and the interface oxidation ratio decreases from ζ/l_d = 15.6 % to ζ/l_d = 9.3 %. At T = 973 K and t = 1 h, the matrix multi-cracking density increases from φ = 0.21/mm at σ_{cr} = 134 MPa to φ = 8.46/mm at σ_{sat} = 178 MPa, and the interface oxidation ratio decreases from ζ/l_d = 15.9 % to ζ/l_d = 9.1 %; and at t = 3 h, the matrix multi-cracking density increases from φ = 0.15/mm at σ_{cr} = 134 MPa to φ = 6.9/mm at σ_{sat} = 186 MPa, and the interface oxidation ratio decreases from ζ/l_d = 38.9 % to ζ/l_d = 24.3 %. At T = 1073 K and t = 1 h, the matrix multi-cracking density increases from φ = 0.14/mm at σ_{cr} = 122 MPa to φ = 6.7/mm at σ_{sat} = 183 MPa, and the interface oxidation ratio decreases from ζ/l_d = 35.7 % to ζ/l_d = 20.7 %; and at t = 3 h, the matrix multi-cracking density increases from φ = 0.09/mm at σ_{cr} = 122 MPa to φ = 4.8/mm at σ_{sat} = 183 MPa, and the interface oxidation ratio decreases from ζ/l_d = 71.5 % to ζ/l_d = 48.2 %.

When V_f = 35 % at T = 873 K and t = 1 h, the matrix multi-cracking density increases from φ = 0.35/mm at σ_{cr} = 180 MPa to φ = 9.75/mm at σ_{sat} = 215 MPa, and the interface oxidation ratio decreases from ζ/l_d = 5.5 % to ζ/l_d = 3.2 %; and at t = 3 h, the matrix multi-cracking density increases from φ = 0.28/mm at σ_{cr} = 180 MPa to φ = 8.9/mm at σ_{sat} = 219 MPa, and the interface oxidation ratio decreases from ζ/l_d = 15.4 % to 9.2 %. At T = 973 K and t = 1 h, the matrix multi-cracking density increases from φ = 0.2/mm at σ_{cr} = 165 MPa to φ = 8.2/mm at σ_{sat} = = 223 MPa, and the interface oxidation ratio decreases from ζ/l_d = 15.9 % to ζ/l_d = 9.2 %; and at t = 3 h, the matrix multi-cracking density increases from φ = 0.15/mm at σ_{cr} = 165 MPa to φ = 6.7/mm at σ_{sat} = 234 MPa, and the interface oxidation ratio decreases from ζ/l_d = 38.8 % to ζ/l_d = 24.3 %. At T = 1073 K and t = 1 h, the matrix multi-cracking density increases from φ = 0.14/mm at σ_{cr} = 148 MPa to φ = 6.6/mm at σ_{sat} = 222 MPa, and the interface oxidation ratio decreases from ζ/l_d = 36 % to ζ/l_d = 21 %; and at t = 3 h, the matrix multi-cracking density increases from φ = 0.09/mm at σ_{cr} = 148 MPa to φ = 4.8/mm at σ_{sat} = 222 MPa, and the interface oxidation ratio decreases from ζ/l_d = 71.9 % to 48.7 %.

Effect of the fibre/matrix interface shear stress

The effect of interface shear stress (i.e., τ_0 = 15, 20 and 25 MPa) on the time-dependent matrix multi-cracking and the fibre/matrix interface oxidation ratio of the SiC/SiC composite at T = 873 K, 973 K and 1073 K for t = 1 h and 3 h are shown in Figure 3.

When τ_0 = 15 MPa at T = 873 K and t = 1 h, the matrix multi-cracking density increases from φ = 0.34/mm at σ_{cr} = 191 MPa to φ = 10.33/mm at σ_{sat} = 234 MPa, and the interface oxidation ratio decreases from ζ/l_d = 6 % to ζ/l_d = 3.5 %; and at t = 3 h, the matrix multi-cracking density increases from φ = 0.27/mm at σ_{cr} = 191 MPa to φ = 9.3/mm at σ_{sat} = 240 MPa, and the interface oxidation ratio decreases from ζ/l_d = 16.6 % to ζ/l_d = 10.2 %. At T = 973 K and t = 1 h, the matrix multi-cracking density increases from φ = 0.21/mm at σ_{cr} = 176 MPa to φ = = 8.7/mm at σ_{sat} = 245 MPa, and the interface oxidation ratio decreases from ζ/l_d = 17.1 % to ζ/l_d = 10.1 %; and at t = 3 h, the matrix multi-cracking density increases from φ = 0.15/mm at σ_{cr} = 176 MPa to φ = 7/mm at σ_{sat} = = 258 MPa, and the interface oxidation ratio decreases from ζ/l_d = 40.6 % to ζ/l_d = 26.3 %. At T = 1073 K and t = 1 h, the matrix multi-cracking density increases from φ = 0.15/mm at σ_{cr} = 159 MPa to φ = 7/mm at σ_{sat} = = 239 MPa, and the interface oxidation ratio decreases from ζ/l_d = 37.5 % to ζ/l_d = 22.8 %; and at t = 3 h, the matrix multi-cracking density increases from φ = 0.09/mm at σ_{cr} = 159 MPa to φ = 4.8/mm at σ_{sat} = 239 MPa, and the interface oxidation ratio decreases from ζ/l_d = 71.7 % to ζ/l_d = 50.9 %.

When τ_0 = 20 MPa at T = 873 K and t = 1 h, the matrix multi-cracking density increases from φ = 0.34/mm at σ_{cr} = 201 MPa to φ = 10.89/mm at σ_{sat} = 251 MPa, and the interface oxidation ratio decreases from ζ/l_d = 6.5 % to ζ/l_d = 3.9 %; and at t = 3 h, the matrix multi-cracking density increases from φ = 0.27/mm at σ_{cr} = 201 MPa to φ = 9.7/mm at σ_{sat} = 260 MPa, and the interface oxidation ratio decreases from ζ/l_d = 17.7 % to ζ/l_d = 11 %. At T = 973 K and t = 1 h, the matrix multi-cracking density increases from φ = 0.22/mm at σ_{cr} = 186 MPa to φ = 9.26/mm at σ_{sat} =265 MPa, and the interface oxidation ratio decreases from ζ/l_d = 18.2 % to ζ/l_d = 11 %; and at t = 3 h, the matrix multi-cracking density increases from φ = 0.15/mm at σ_{cr} = 186 MPa to φ = 7.3/mm at σ_{sat} = 280 MPa, and the interface oxidation ratio decreases from ζ/l_d = 42.3 % to ζ/l_d = 28.1 %. At T = 1073 K and t = 1 h, the matrix multi-cracking density increases from φ = 0.15/mm at σ_{cr} = 169 MPa to φ = 7.4/mm at σ_{sat} = 254 MPa, and the interface oxidation ratio decreases from ζ/l_d = 39 % to ζ/l_d = 24.5 %; and at t = 3 h, the matrix multi-cracking density increases from φ = 0.09/mm at σ_{cr} = 169 MPa to φ = 4.9/mm at σ_{sat} = 254 MPa, and the interface oxidation ratio decreases from ζ/l_d = 72.1 % to ζ/l_d = 52.9 %.

When τ_0 = 25 MPa at T = 873 K and t = 1 h, the matrix multi-cracking density increases from φ = 0.35/mm at σ_{cr} = 211 MPa to φ = 11.4/mm at σ_{sat} = 270 MPa, and the interface oxidation ratio decreases from ζ/l_d = 7 % to ζ/l_d = 4.2 %; and at t = 3 h, the matrix multi-cracking density increases from φ = 0.28/mm at σ_{cr} = 211 MPa to φ = 10.2/mm at σ_{sat} = 277 MPa, and the interface oxidation ratio decreases from ζ/l_d = 18.8 % to ζ/l_d = 11.8 %.

At T = 973 K and t = 1 h, the matrix multi-cracking density increases from φ = 0.23/mm at σ_{cr} = 195 MPa to φ = 9.7/mm at σ_{sat} = 282 MPa, and the interface oxidation ratio decreases from ζ/l_d = 19.3 % to ζ/l_d = 11.8 %; and at t = 3 h, the matrix multi-cracking density increases from φ = 0.15/mm at σ_{cr} = 195 MPa to φ = 7.5/mm at σ_{sat} = 293 MPa, and the interface oxidation ratio decreases from ζ/l_d = 43.8 % to ζ/l_d = 29.7 %. At T = 1073 K

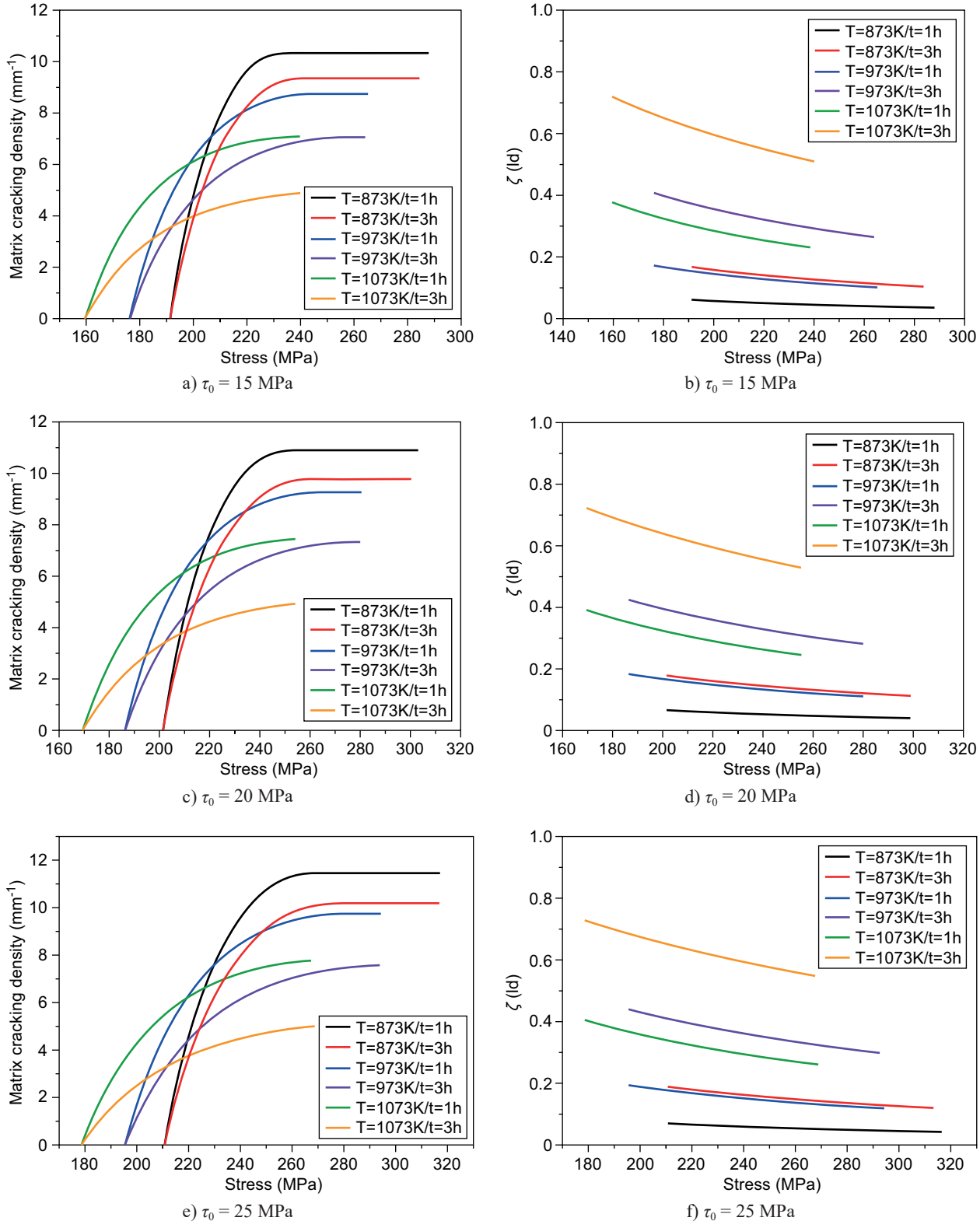

a) τ_0 = 15 MPa b) τ_0 = 15 MPa

c) τ_0 = 20 MPa d) τ_0 = 20 MPa

e) τ_0 = 25 MPa f) τ_0 = 25 MPa

Figure 3. The matrix cracking density versus the applied stress curves for the different oxidation temperature and time when τ_0 = 15 MPa (a), 20 MPa (c), 25 MPa (e); the interface oxidation ratio versus the applied stress curves for the different oxidation temperature and time when τ_0 = 15 MPa (b), 20 MPa (d), 25 MPa (f).

and t = 1 h, the matrix multi-cracking density increases from φ = 0.16/mm at σ_{cr} = 178 MPa to φ = 7.7/mm at σ_{sat} = 268 MPa, and the interface oxidation ratio decreases from ζ/l_d = 40.4 % to ζ/l_d = 26.1 %; and at t = 3 h, the matrix multi-cracking density increases from φ = 0.09/mm at σ_{cr} = 178 MPa to φ = 5/mm at σ_{sat} = 268 MPa, and the interface oxidation ratio decreases from ζ/l_d = 72.6 % to ζ/l_d = 54.6 %.

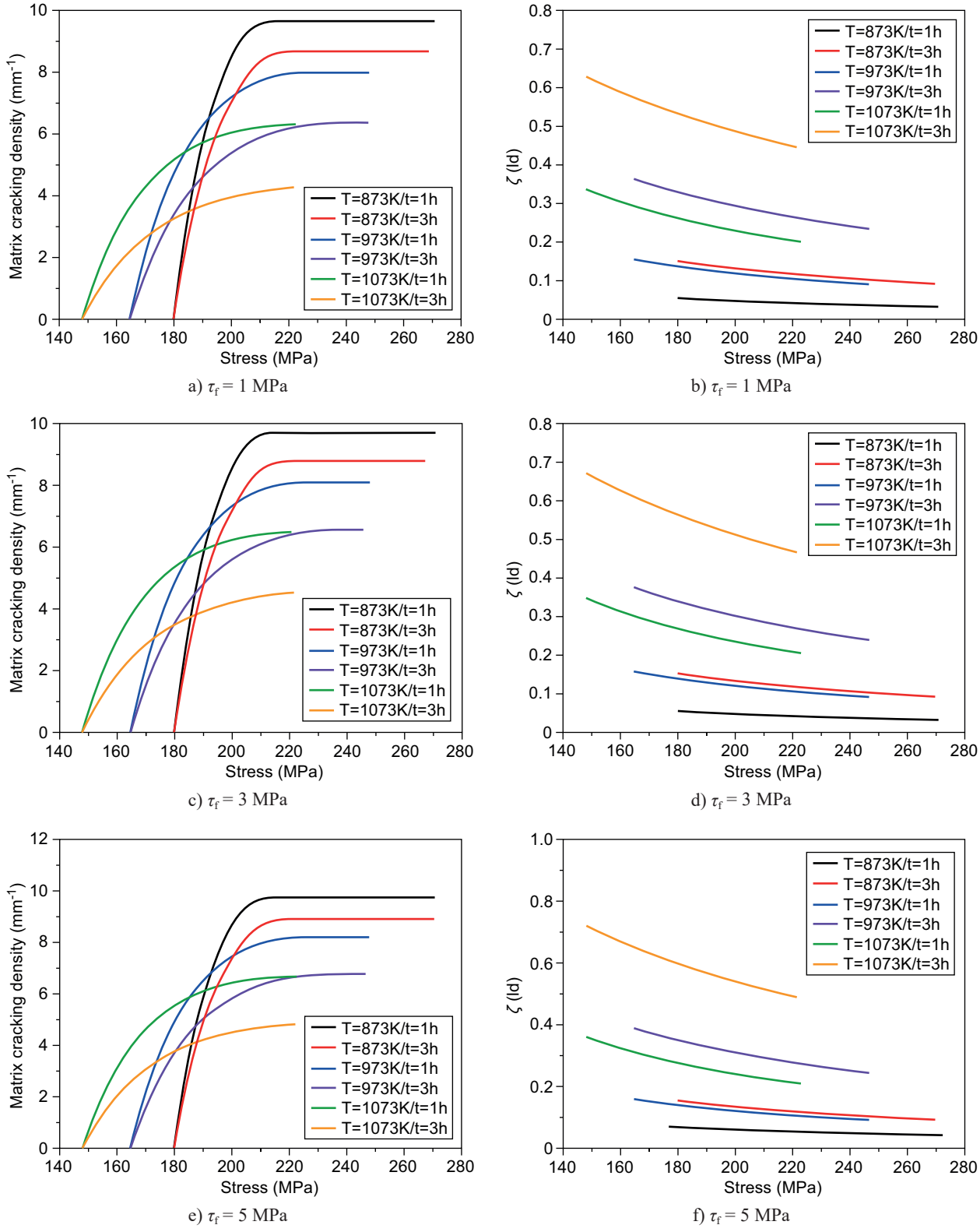

a) τ_f = 1 MPa

b) τ_f = 1 MPa

c) τ_f = 3 MPa

d) τ_f = 3 MPa

e) τ_f = 5 MPa

f) τ_f = 5 MPa

Figure 4. The matrix cracking density versus the applied stress curves for the different oxidation temperature and time when τ_f = 1 MPa (a), 3 MPa (c), 5 MPa (e); the interface oxidation ratio versus the applied stress curves for the different oxidation temperature and time when τ_f = 1 MPa (b), 3 MPa (d), 5 MPa (f).

The effect of interface shear stress (i.e., τ_f = 1, 3 and 5 MPa) on the time-dependent matrix multi-cracking and the fibre/matrix interface oxidation of the SiC/SiC composite at T = 873 K, 973 K and 1073 K for t = 1 h and 3 h are shown in Figure 4.

When τ_f = 1 MPa at T = 873 K and t = 1 h, the matrix multi-cracking density increases from φ = 0.34/mm at σ_{cr} = 180 MPa to φ = 9.6/mm at σ_{sat} = 214 MPa, and the interface oxidation ratio decreases from ζ/l_d = 5.5 % to ζ/l_d = 3.2 %; and at t = 3 h, the matrix multi-cracking density increases from φ = 0.27/mm at σ_{cr} = 180 MPa to φ = 8.6/mm at σ_{sat} = 220 MPa, and the interface oxidation ratio decreases from ζ/l_d = 15 % to ζ/l_d = 9.1 %. At T = 973 K and t = 1 h, the matrix multi-cracking density increases from φ = 0.19/mm at σ_{cr} = 165 MPa to φ = = 7.9/mm at σ_{sat} = 225 MPa, and the interface oxidation ratio decreases from ζ/l_d = 15.4 % to ζ/l_d = 9 %; and at t = 3 h, the matrix multi-cracking density increases from φ = 0.13/mm at σ_{cr} = 165 MPa to φ = 6.3/mm at σ_{sat} = = 237 MPa, and the interface oxidation ratio decreases from ζ/l_d = 36.2 % to ζ/l_d = 23.3 %. At T = 1073 K and t = 1 h, the matrix multi-cracking density increases from φ = 0.13/mm at σ_{cr} = 148 MPa to φ = 6.3/mm at σ_{sat} = = 222 MPa, and the interface oxidation ratio decreases from ζ/l_d = 33.5 % to ζ/l_d = 20 %; and at t = 3 h, the matrix multi-cracking density increases from φ = 0.07/mm at σ_{cr} = 148 MPa to φ = 4.2/mm at σ_{sat} = 222 MPa, and the interface oxidation ratio decreases from ζ/l_d = 62.7 % to ζ/l_d = 44.3 %.

When τ_f = 3 MPa at T = 873 K and t = 1 h, the matrix multi-cracking density increases from φ = 0.35/mm at σ_{cr} = 180 MPa to φ = 9.7/mm at σ_{sat} = 214 MPa, and the interface oxidation ratio decreases from ζ/l_d = 5.5 % to ζ/l_d = 3.2 %; and at t = 3 h, the matrix multi-cracking density increases from φ = 0.28/mm at σ_{cr} = 180 MPa to φ = 8.7/mm at σ_{sat} =220 MPa, and the interface oxidation ratio decreases from ζ/l_d = 15.2 % to ζ/l_d = 9.2 %. At T = 973 K and t = 1 h, the matrix multi-cracking density increases from φ = 0.2/mm at σ_{cr} = 165 MPa to φ = = 8.0/mm at σ_{sat} = 224 MPa, and the interface oxidation ratio decreases from ζ/l_d = 15.6 % to ζ/l_d = 9.1 %; and at t = 3 h, the matrix multi-cracking density increases from φ = 0.14/mm at σ_{cr} = 165 MPa to φ = 6.5/mm at σ_{sat} = 236 MPa, and the interface oxidation ratio decreases from ζ/l_d = 37.5 % to ζ/l_d = 23.8 %. At T = 1073 K and t = 1 h, the matrix multi-cracking density increases from φ = 0.14/mm at σ_{cr} = 148 MPa to φ = 6.4/mm at σ_{sat} = 222 MPa, and the interface oxidation ratio decreases from ζ/l_d = 34.7 % to ζ/l_d = 20.5 %; and at t = 3 h, the matrix multi-cracking density increases from φ = 0.08/mm at σ_{cr} = 148 MPa to φ = 4.5/mm at σ_{sat} = 222 MPa, and the interface oxidation ratio decreases from ζ/l_d = 67 % to ζ/l_d = 46.4 %.

When τ_f = 5 MPa at T = 873 K and t = 1 h, the matrix multi-cracking density increases from φ = 0.35/mm at σ_{cr} = 180 MPa to φ = 9.7/mm at σ_{sat} = 214 MPa, and the interface oxidation ratio decreases from ζ/l_d = 5.5 % to ζ/l_d = 3.2 %; and at t = 3 h, the matrix multi-cracking density increases from φ = 0.29/mm at σ_{cr} =180 MPa to φ = 8.9/mm at σ_{sat} = 220 MPa, and the interface oxidation ratio decreases from ζ/l_d = 15.4 % to ζ/l_d = 9.3 %. At T = 973 K and t = 1 h, the matrix multi-cracking density increases from φ = 0.2/mm at σ_{cr} = 165 MPa to φ = 8.2/mm at σ_{sat} = 224 MPa, and the interface oxidation ratio decreases from ζ/l_d = 15.9 % to ζ/l_d = 9.2 %; and at t = 3 h, the matrix multi-cracking density increases from φ = 0.15/mm at σ_{cr} = 165 MPa to φ = 6.7/mm at σ_{sat} = 234 MPa, and the interface oxidation ratio decreases from ζ/l_d = 38.8 % to ζ/l_d = 24.3 %. At T = 1073 K and t = 1 h, the matrix multi-cracking density increases from φ = 0.15/mm at σ_{cr} =148 MPa to φ = 6.6/mm at σ_{sat} = 222 MPa, and the interface oxidation ratio decreases from ζ/l_d = 36 % to ζ/l_d = 21 %; and at t = 3 h, the matrix multi-cracking density increases from φ = 0.09/mm at σ_{cr} = 148 MPa to φ = 4.8/mm at σ_{sat} = 222 MPa, and the interface oxidation ratio decreases from ζ/l_d = 72 % to ζ/l_d = 48.7 %.

Effect of the fibre/matrix interface frictional coefficient

The effect of the fibre/matrix interface frictional coefficient (i.e., μ = 0.05, 0.1 and 0.15) on the time-dependent matrix multi-cracking and the fibre/matrix interface oxidation ratio of the SiC/SiC composite at T = 873 K, 973 K and 1073 K for t = 1 h and 3 h are shown in Figure 5.

When μ = 0.05 at T = 873 K and t = 1 h, the matrix multi-cracking density increases from φ = 1.2/mm at σ_{cr} = 128 MPa to φ = 9.9/mm at σ_{sat} = 136 MPa, and the interface oxidation ratio decreases from ζ/l_d = 4.9 % to ζ/l_d = 2.7 %; and at t = 3 h, the matrix multi-cracking density increases from φ = 0.71/mm at σ_{cr} = 128 MPa to φ = 9.2/mm at σ_{sat} = 138 MPa, and the interface oxidation ratio decreases from ζ/l_d = 13.8 % to ζ/l_d = 7.9 %. At T = 973 K and t = 1 h, the matrix multi-cracking density increases from φ = 0.21/mm at σ_{cr} = 120 MPa to φ = 7.9/mm at σ_{sat} = 151 MPa, and the interface oxidation ratio decreases from ζ/l_d = 14.5 % to ζ/l_d = 7.9 %; and at t = 3 h, the matrix multi-cracking density increases from φ = 0.16/mm at σ_{cr} = 120 MPa to φ = 6.7/mm at σ_{sat} = 156 MPa, and the interface oxidation ratio decreases from ζ/l_d = 37.1 % to ζ/l_d = 21.7 %. At T = 1073 K and t = 1 h, the matrix multi-cracking density increases from φ = 0.14/mm at σ_{cr} = 110 MPa to φ = 6.3/mm at σ_{sat} = = 162 MPa, and the interface oxidation ratio decreases from ζ/l_d = 34.8 % to ζ/l_d = 18.8 %; and at t = 3 h, the matrix multi-cracking density increases from φ = 0.09/mm at σ_{cr} = 110 MPa to φ = 4.8/mm at σ_{sat} = 166 MPa, and the interface oxidation ratio decreases from ζ/l_d = 73.7 % to ζ/l_d = 46.1 %.

When μ = 0.1 at T = 873 K and t = 1 h, the matrix multi-cracking density increases from φ = 0.47/mm at σ_{cr} = 146 MPa to φ = 10.3/mm at σ_{sat} = 167 MPa, and the

interface oxidation ratio decreases from ζ/l_d = 5.6 % to ζ/l_d = 3.2 %; and at t = 3 h, the matrix multi-cracking density increases from φ = 0.35/mm at σ_{cr} = 146 MPa to φ = 9.4/mm at σ_{sat} = 170 MPa, and the interface oxidation ratio decreases from ζ/l_d = 15.6 % to ζ/l_d = 9.3 %. At T = 973 K and t = 1 h, the matrix multi-cracking density increases from φ = 0.21/mm at σ_{cr} = 134 MPa to φ = 8.4/mm at σ_{sat} = 178 MPa, and the interface oxidation

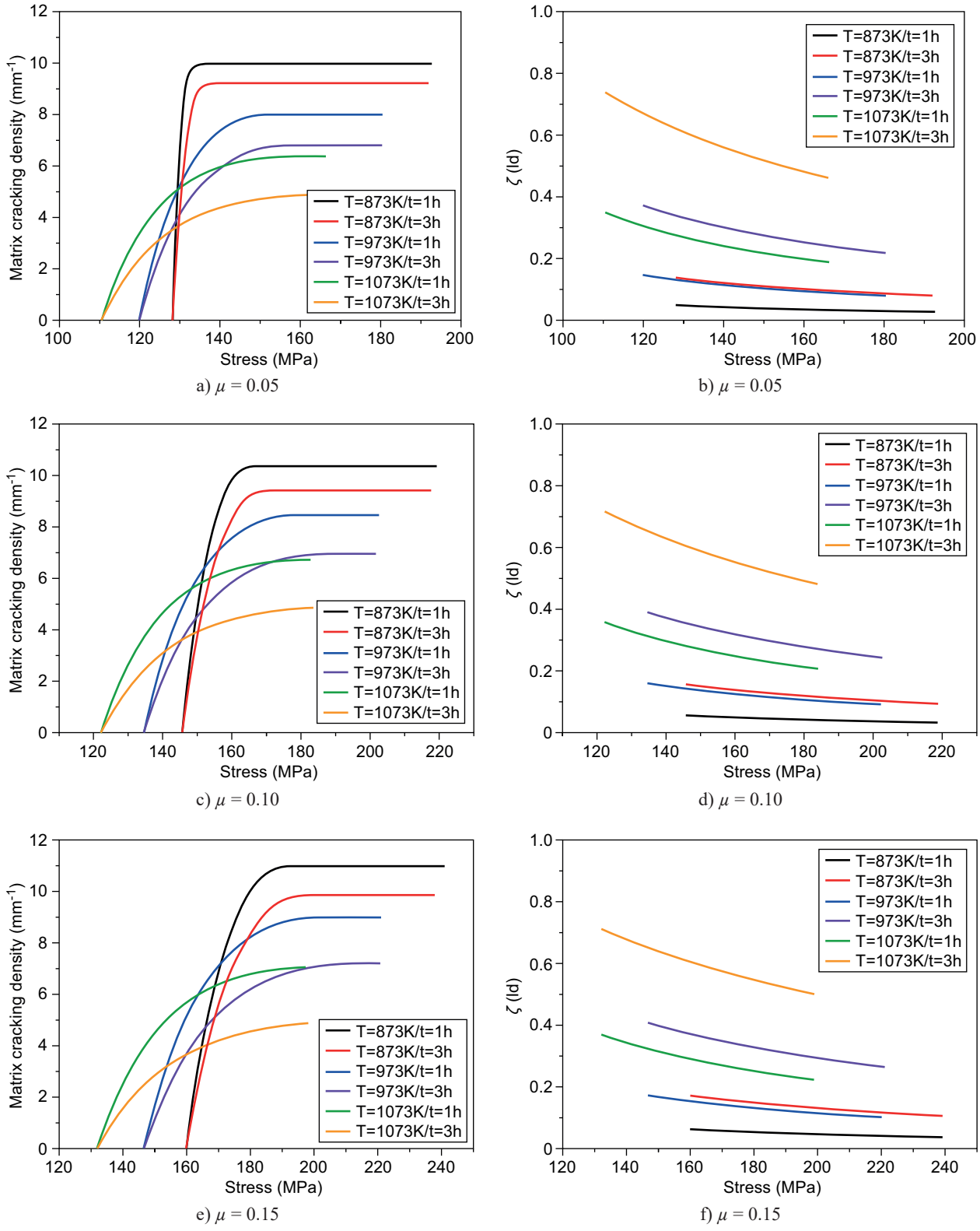

a) μ = 0.05 b) μ = 0.05

c) μ = 0.10 d) μ = 0.10

e) μ = 0.15 f) μ = 0.15

Figure 5. The matrix cracking density versus the applied stress curves for the different oxidation temperature and time when μ = 0.05 (a), 0.10 (c), 0.15 (e); the interface oxidation ratio versus the applied stress curves for the different oxidation temperature and time when μ = 0.05 (b), 0.10 (d), 0.15 (f).

ratio decreases from ζ/l_d = 15.9 % to ζ/l_d = 9.1 %; and at t = 3 h, the matrix multi-cracking density increases from φ = 0.15/mm at σ_{cr} = 134 MPa to φ = 6.9/mm at σ_{sat} = 186 MPa, and the interface oxidation ratio decreases from ζ/l_d = 38.9 % to ζ/l_d = 24.3 %. At T = 1073 K and t = 1 h, the matrix multi-cracking density increases from φ = 0.14/mm at σ_{cr} = 122 MPa to φ = 6.7/mm at σ_{sat} = = 183 MPa, and the interface oxidation ratio decreases from ζ/l_d = 35.7 % to ζ/l_d = 20.7 %; and at t = 3 h, the matrix multi-cracking density increases from φ = 0.09/mm at σ_{cr} = 122 MPa to φ = 4.8/mm at σ_{sat} = 183 MPa, and the interface oxidation ratio decreases from ζ/l_d = 71.5 % to ζ/l_d = 48.2 %.

When μ = 0.15 at T = 873 K and t = 1 h, the matrix multi-cracking density increases from φ = 0.4/mm at σ_{cr} = 160 MPa to φ = 10.9/mm at σ_{sat} = 193 MPa, and the interface oxidation ratio decreases from ζ/l_d = 6.3 % to ζ/l_d = 3.7 %; and at t = 3 h, the matrix multi-cracking density increases from φ = 0.31/mm at σ_{cr} = 160 MPa to φ = 9.8/mm at σ_{sat} = 198 MPa, and the interface oxidation ratio decreases from ζ/l_d = 17.1 % to ζ/l_d = 10.5 %. At T = 973 K and t = 1 h, the matrix multi-cracking density increases from φ = 0.22/mm at σ_{cr} = 147 MPa to φ = 8.9/mm at σ_{sat} = 201 MPa, and the interface oxidation ratio decreases from ζ/l_d = 17.2 % to ζ/l_d = 10.2 %; and at t = 3 h, the matrix multi-cracking density increases from φ = 0.15/mm at σ_{cr} = 147 MPa to φ = 7.2/mm at σ_{sat} = 212MPa, and the interface oxidation ratio decreases from ζ/l_d = 40.7 % to ζ/l_d = 26.5 %. At T = 1073 K and t = 1 h, the matrix multi-cracking density increases from φ = 0.15/mm at σ_{cr} = 132 MPa to φ = 7/mm at σ_{sat} = 198 MPa, and the interface oxidation ratio decreases from ζ/l_d = 36.9 % to ζ/l_d = 22.4 %; and at t = 3 h, the matrix multi-cracking density increases from φ = = 0.09/mm at σ_{cr} = 132 MPa to φ = 4.8/mm at σ_{sat} = = 198MPa, and the interface oxidation ratio decreases from ζ/l_d = 71 % to ζ/l_d = 50.1 %.

Effect of the fibre/matrix interface de-bonded energy

The effect of the fibre/matrix interface de-bonded energy (i.e., γ_d = 0.3, 0.5 and 0.7 J·m^{-2}) on the time-dependent matrix multi-cracking and the fibre/matrix interface oxidation ratio of the SiC/SiC composite at T = 873 K, 973 K and 1073 K for t = 1 h and 3 h are shown in Figure 6.

When γ_d = 0.3 J·m^{-2} at T = 873 K and t = 1 h, the matrix multi-cracking density increases from φ = 0.7/mm at σ_{cr} = 146 MPa to φ = 10.3/mm at σ_{sat} = 160 MPa, and the interface oxidation ratio decreases from ζ/l_d = 5.2 % to ζ/l_d = 3.1 %; and at t = 3 h, the matrix multi-cracking density increases from φ = 0.49/mm at σ_{cr} = 146 MPa to φ = 9.4/mm at σ_{sat} = 164 MPa, and the interface oxidation ratio decreases from ζ/l_d = 14.7 % to ζ/l_d = 9.0 %. At T = 973 K and t = 1 h, the matrix multi-cracking density increases from φ = 0.24/mm at σ_{cr} = 134 MPa to φ = 8.4/mm at σ_{sat} = 171 MPa, and the interface oxidation ratio decreases from ζ/l_d = 14.7 % to ζ/l_d = 8.7 %; and at t = 3 h, the matrix multi-cracking density increases from φ = 0.16/mm at σ_{cr} = 134 MPa to φ = 6.9/mm at σ_{sat} = 179 MPa, and the interface oxidation ratio decreases from ζ/l_d = 36.5 % to ζ/l_d = 23.3 %. At T = 1073 K and t = 1 h, the matrix multi-cracking density increases from φ = 0.15/mm at σ_{cr} = 122 MPa to φ = 6.7/mm at σ_{sat} = 183 MPa, and the interface oxidation ratio decreases from ζ/l_d = 32.6 % to ζ/l_d = 19.6 %; and at t = 3 h, the matrix multi-cracking density increases from φ = 0.09/mm at σ_{cr} = 122 MPa to φ = 4.8/mm at σ_{sat} = 183 MPa, and the interface oxidation ratio decreases from ζ/l_d = 67.3 % to ζ/l_d = 46.3 %.

When γ_d = 0.5 J·m^{-2} at T = 873 K and t = 1 h, the matrix multi-cracking density increases from φ = 0.3/mm at σ_{cr} = 146 MPa to φ = 10.3/mm at σ_{sat} = 173 MPa, and the interface oxidation ratio decreases from ζ/l_d = 5.9 % to ζ/l_d = 3.3 %; and at t = 3 h, the matrix multi-cracking density increases from φ = 0.29/mm at σ_{cr} = 146 MPa to φ = 9.4/mm at σ_{sat} = 176 MPa, and the interface oxidation ratio decreases from ζ/l_d = 16.5 % to ζ/l_d = 9.6 %. At T = 973 K and t = 1 h, the matrix multi-cracking density increases from φ = 0.2/mm at σ_{cr} = 134 MPa to φ = = 8.4/mm at σ_{sat} = 184 MPa, and the interface oxidation ratio decreases from ζ/l_d = 17.1 % to ζ/l_d = 9.5 %; and at t = 3 h, the matrix multi-cracking density increases from φ = 0.15/mm at σ_{cr} = 134 MPa to φ = 6.9/mm at σ_{sat} = 192 MPa, and the interface oxidation ratio decreases from ζ/l_d = 41.2 % to ζ/l_d = 25.2 %. At T = 1073 K and t = 1 h, the matrix multi-cracking density increases from φ = 0.15/mm at σ_{cr} = 122 MPa to φ = 6.7/mm at σ_{sat} = 183 MPa, and the interface oxidation ratio decreases from ζ/l_d = 38.9 % to ζ/l_d = 21.7 %; and at t = 3 h, the matrix multi-cracking density increases from φ = 0.09/mm at σ_{cr} = 122 MPa to φ = 4.8/mm at σ_{sat} = 183 MPa, and the interface oxidation ratio decreases from ζ/l_d = 75.6 % to ζ/l_d = 50 %.

When γ_d = 0.7 J·m^{-2} at T = 873 K and t = 1 h, the matrix multi-cracking density increases from φ = 0.3/mm at σ_{cr} =146 MPa to φ = 10.3/mm at σ_{sat} = 183 MPa, and the interface oxidation ratio decreases from ζ/l_d = 6.7 % to ζ/l_d = 3.6 %; and at t = 3 h, the matrix multi-cracking density increases from φ = 0.24/mm at σ_{cr} = 146 MPa to φ = 9.4/mm at σ_{sat} = 186 MPa, and the interface oxidation ratio decreases from ζ/l_d = 18.2 % to ζ/l_d = 10.2 %. At T = 973 K and t = 1 h, the matrix multi-cracking density increases from φ = 0.2/mm at σ_{cr} = 134 MPa to φ = 8.4/mm at σ_{sat} = 202 MPa, and the interface oxidation ratio decreases from ζ/l_d = 19.7 % to ζ/l_d = 10.3 %; and at t = 3 h, the matrix multi-cracking density increases from φ = 0.15/mm at σ_{cr} = 134 MPa to φ = 6.9/mm at σ_{sat} = 202 MPa, and the interface oxidation ratio decreases from ζ/l_d = 46 % to ζ/l_d = 27 %. At T = 1073 K and t = 1 h, the matrix multi-cracking density increases from

φ = 0.16/mm at σ_{cr} = 122 MPa to φ = 6.8/mm at σ_{sat} = = 183 MPa, and the interface oxidation ratio decreases from ζ/l_d = 46 % to ζ/l_d = 23.8 %; and at t = 3 h, the matrix multi-cracking density increases from φ = 0.09/mm at σ_{cr} = 122 MPa to φ = 4.9/mm at σ_{sat} = 183 MPa, and the interface oxidation ratio decreases from ζ/l_d = 84.1 % to ζ/l_d = 53.6 %.

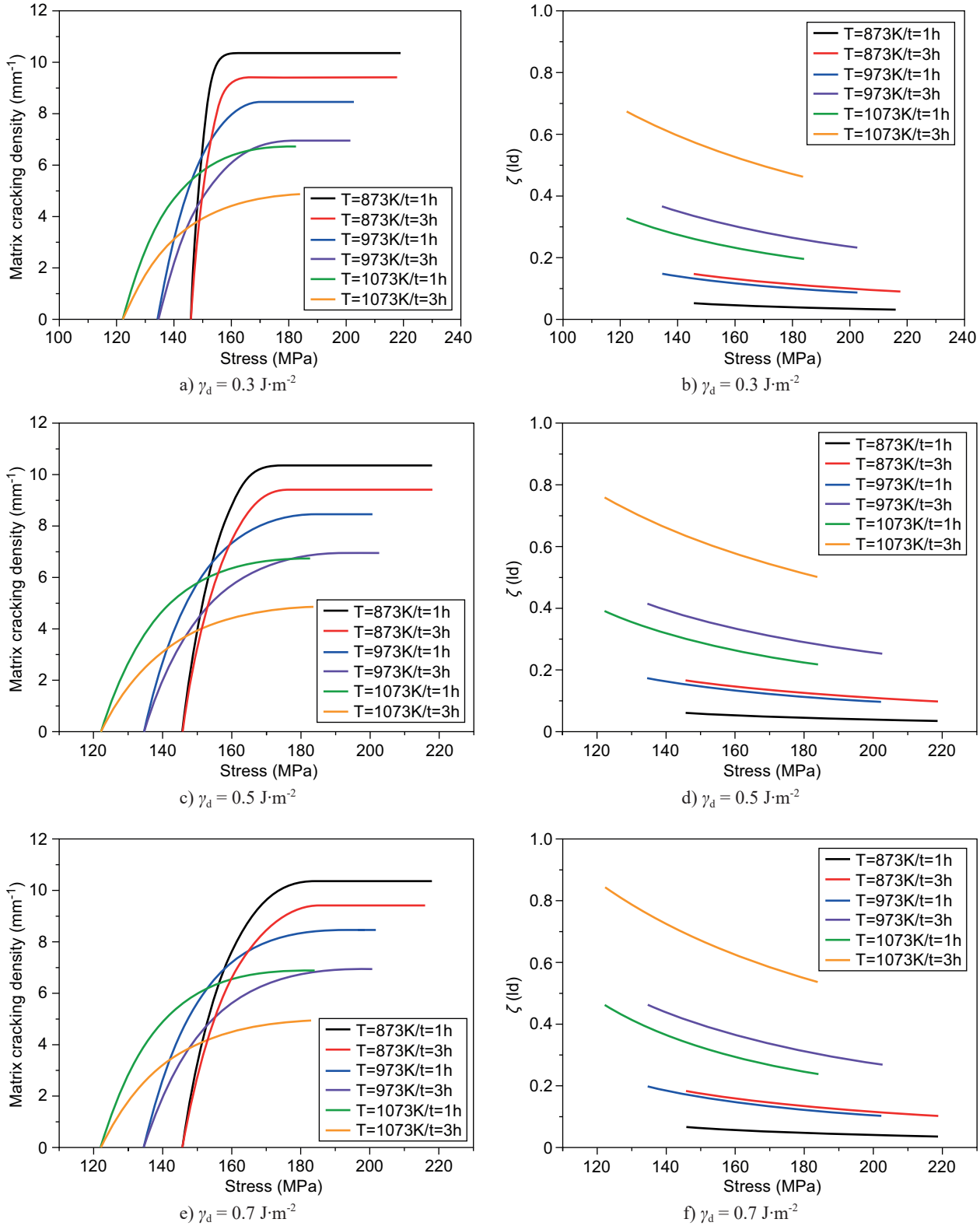

a) γ_d = 0.3 J·m^{-2} b) γ_d = 0.3 J·m^{-2}

c) γ_d = 0.5 J·m^{-2} d) γ_d = 0.5 J·m^{-2}

e) γ_d = 0.7 J·m^{-2} f) γ_d = 0.7 J·m^{-2}

Figure 6. The matrix cracking density versus the applied stress curves for the different oxidation temperature and time when γ_d = 0.3 J·m^{-2} (a), 0.5 J·m^{-2} (c), 0.7 J·m^{-2} (e); the interface oxidation ratio versus the applied stress curves for the different oxidation temperature and time when γ_d = 0.3 J·m^{-2} (b), 0.5 J·m^{-2} (d), 0.7 J·m^{-2} (f).

Effect of the matrix fracture energy

The effect of the matrix fracture energy (i.e., $\gamma_m = 20$, 25 and 30 J·m^{-2}) on the time-dependent matrix multi-cracking and the fibre/matrix interface oxidation ratio of the SiC/SiC composite at $T = 873$ K, 973 K and 1073 K for $t = 1$ h and 3 h are shown in Figure 7.

When $\gamma_m = 20$ J·m^{-2} at $T = 873$ K and $t = 1$ h, the matrix multi-cracking density increases from $\varphi = 0.3$/mm

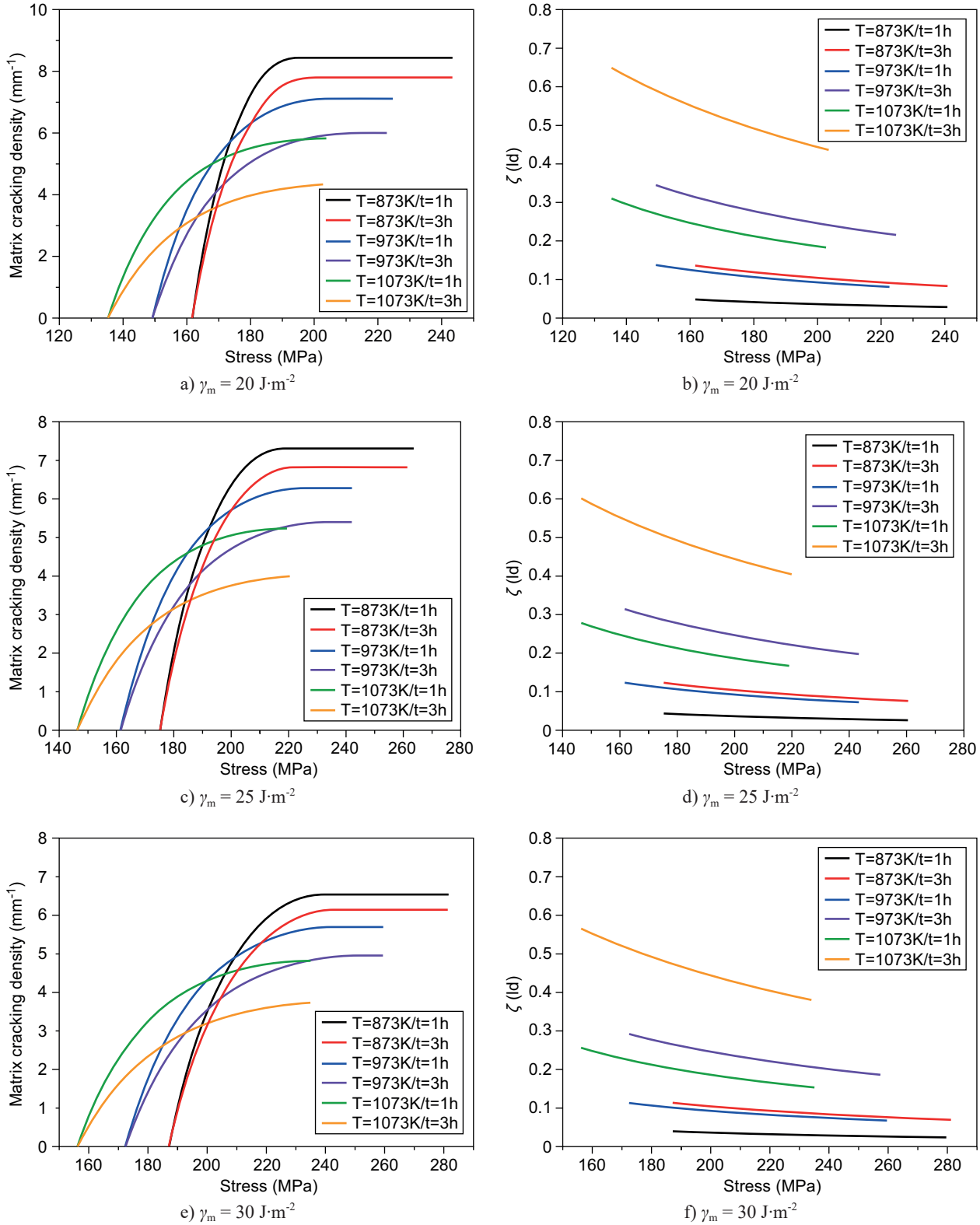

a) $\gamma_m = 20$ J·m^{-2} b) $\gamma_m = 20$ J·m^{-2}

c) $\gamma_m = 25$ J·m^{-2} d) $\gamma_m = 25$ J·m^{-2}

e) $\gamma_m = 30$ J·m^{-2} f) $\gamma_m = 30$ J·m^{-2}

Figure 7. The matrix cracking density versus the applied stress curves for the different oxidation temperature and time when $\gamma_m = 20$ J·m^{-2} (a), 25 J·m^{-2} (c), 30 J·m^{-2} (e); the interface oxidation ratio versus the applied stress curves for the different oxidation temperature and time when $\gamma_m = 20$ J·m^{-2} (b), 25 J·m^{-2} (d), 30 J·m^{-2} (f).

at σ_{cr} = 162 MPa to φ = 8.4/mm at σ_{sat} = 195 MPa, and the interface oxidation ratio decreases from ζ/l_d = 4.8% to ζ/l_d = 2.8 %; and at t = 3 h, the matrix multi-cracking density increases from φ = 0.24/mm at σ_{cr} = 162 MPa to φ = 7.8/mm at σ_{sat} = 199 MPa, and the interface oxidation ratio decreases from ζ/l_d = 13.6 % to ζ/l_d = 8.2 %. At T = 973 K and t = 1 h, the matrix multi-cracking density increases from φ = 0.18/mm at σ_{cr} =149 MPa to φ = 7.1/mm at σ_{sat} = 204 MPa, and the interface oxidation ratio decreases from ζ/l_d = 13.7 % to ζ/l_d = 8 %; and at t = 3 h, the matrix multi-cracking density increases from φ = 0.13/mm at σ_{cr} = 149 MPa to φ = 6/mm at σ_{sat} = 212 MPa, and the interface oxidation ratio decreases from ζ/l_d = 34.4 % to ζ/l_d = 21.6 %. At T = 1073 K and t = 1 h, the matrix multi-cracking density increases from φ = 0.13/mm at σ_{cr} = 135 MPa to φ = 5.8/mm at σ_{sat} = = 203 MPa, and the interface oxidation ratio decreases from ζ/l_d = 30.9 % to ζ/l_d = 18.2 %; and at t = 3 h, the matrix multi-cracking density increases from φ = 0.08/mm at σ_{cr} = 135 MPa to φ = 4.3/mm at σ_{sat} = 203 MPa, and the interface oxidation ratio decreases from ζ/l_d = 64.7 % to ζ/l_d = 43.6 %.

When γ_m = 25 J·m^{-2} at T = 873 K and t = 1 h, the matrix multi-cracking density increases from φ = 0.23/mm at σ_{cr} = 175 MPa to φ = 7.3/mm at σ_{sat} = 218 MPa, and the interface oxidation ratio decreases from ζ/l_d = 4.3 % to ζ/l_d = 2.6 %; and at t = 3 h, the matrix multi-cracking density increases from φ = 0.2/mm at σ_{cr} = 175 MPa to φ = 6.8/mm at σ_{sat} = 222 MPa, and the interface oxidation ratio decreases from ζ/l_d = 12.2 % to ζ/l_d = 7.5 %. At T = 973 K and t = 1 h, the matrix multi-cracking density increases from φ = 0.15/mm at σ_{cr} = 162 MPa to φ = 6.2/mm at σ_{sat} = 243 MPa, and the interface oxidation ratio decreases from ζ/l_d = 12.3 % to ζ/l_d = 7.3 %; and at t = 3 h, the matrix multi-cracking density increases from φ = 0.12/mm at σ_{cr} = 162 MPa to φ = 5.4/mm at σ_{sat} = 234 MPa, and the interface oxidation ratio decreases from ζ/l_d = 31.3 % to ζ/l_d = 19.8 %. At T = 1073 K and t = 1 h, the matrix multi-cracking density increases from φ = 0.12/mm at σ_{cr} = 146 MPa to φ = 5.2/mm at σ_{sat} = 220 MPa, and the interface oxidation ratio decreases from ζ/l_d = 27.7 % to ζ/l_d = 16.5 %; and at t = 3 h, the matrix multi-cracking density increases from φ = 0.08/mm at σ_{cr} = 146 MPa to φ = 4.0/mm at σ_{sat} = 220 MPa, and the interface oxidation ratio decreases from ζ/l_d = 60 % to ζ/l_d = 40.4 %.

When γ_m = 30 J·m^{-2} at T = 873 K and t = 1 h, the matrix multi-cracking density increases from φ = 0.2/mm at σ_{cr} = 187 MPa to φ = 6.5/mm at σ_{sat} = 239 MPa, and the interface oxidation ratio decreases from ζ/l_d = 4 % to ζ/l_d = 2.4 %; and at t = 3 h, the matrix multi-cracking density increases from φ = 0.17/mm at σ_{cr} = 167 MPa to φ = 6.1/mm at σ_{sat} = 242 MPa, and the interface oxidation ratio decreases from ζ/l_d = 11.3 % to ζ/l_d = 6.9 %. At T = 973 K and t = 1 h, the matrix multi-cracking density increases from φ = 0.14/mm at σ_{cr} = 172 MPa to φ = 5.6/mm at σ_{sat} = 243 MPa, and the interface oxidation ratio decreases from ζ/l_d = 11.2 % to ζ/l_d = 6.7 %; and at t = 3 h, the matrix multi-cracking density increases from φ = 0.11/mm at σ_{cr} = 172 MPa to φ = 4.9/mm at σ_{sat} = 253 MPa, and the interface oxidation ratio decreases from ζ/l_d = 29.1 % to ζ/l_d = 18.4 %. At T = 1073 K and t = 1 h, the matrix multi-cracking density increases from φ = 0.11/mm at σ_{cr} = 156 MPa to φ = 4.8/mm at σ_{sat} = = 234 MPa, and the interface oxidation ratio decreases from ζ/l_d = 25.4 % to ζ/l_d = 15.3 %; and at t = 3 h, the matrix multi-cracking density increases from φ = 0.07/mm at σ_{cr} = 156 MPa to φ = 3.7/mm at σ_{sat} = 234 MPa, and the interface oxidation ratio decreases from ζ/l_d = 56.3 % to ζ/l_d = 37.9 %.

EXPERIMENTAL COMPARISONS

The experimental and theoretical matrix multi-cracking density and the fibre/matrix interface oxidation ratio of the unidirectional SiC/SiC [29] and mini SiC/SiC [30] composites composite at room temperature, T = 773 K, 873 K, 973 K and 1073 K for t = 1 h and 3 h are predicted, as shown in Figures 8 and 9.

The unidirectional SiC/SiC composite

Beyerle et al. [29] investigated the damage evolution of the matrix multi-cracking in the unidirectional SiC/SiC composite. At room temperature, the matrix multi-cracking evolution starts at σ_{cr} = 240 MPa and approaches saturation at σ_{sat} = 320 MPa; and the matrix cracking density increases from φ = 1.1/mm to φ = 13/mm.

At T = 773 K, the matrix multi-cracking density increases from φ = 0.5/mm at σ_{cr} = 222 MPa to φ = 12.4/mm at σ_{sat} = 311 MPa; at T = 773 K and t = 1 h, the matrix multi-cracking density increases from φ = 0.36/mm at σ_{cr} = 222 MPa to φ = 11.9/mm at σ_{sat} = 272 MPa, and the interface oxidation ratio decreases from ζ/l_d = 2 % at σ_{cr} = 222 MPa to ζ/l_d = 1.1 % at σ_{sat} = 272 MPa; and at T = 773 K and t = 3 h, the matrix multi-cracking density increases from φ = 0.34/mm at σ_{cr} = 222 MPa to φ = 11.5/mm at σ_{sat} = 273 MPa, and the interface oxidation ratio decreases from ζ/l_d = 5.8 % at σ_{cr} = 222 MPa to ζ/l_d = 3.4 % at σ_{sat} = 273 MPa.

At T = 873 K, the matrix multi-cracking density increases from φ = 0.45/mm at σ_{cr} = 206 MPa to φ = = 11.2/mm at σ_{sat} = 288 MPa; at T = 873 K and t = 1 h, the matrix multi-cracking density increases from φ = 0.25/mm at σ_{cr} = 206 MPa to φ = 10.3/mm at σ_{sat} = 288 MPa, and the interface oxidation ratio decreases from ζ/l_d = 8.3 % at σ_{cr} = 206 MPa to ζ/l_d = 4.6 % at σ_{sat} = 288 MPa; and at T = 873 K and t = 3 h, the matrix multi-cracking density increases from φ = 0.21/mm at σ_{cr} = 206 MPa to φ = 9.4/mm at σ_{sat} = 288 MPa, and the interface oxidation ratio decreases from ζ/l_d = 22.3 % at σ_{cr} = 206 MPa to ζ/l_d = 13 % at σ_{sat} = 288 MPa.

At T = 973 K, the matrix multi-cracking density increases from φ = 0.4/mm at σ_{cr} = 188 MPa to φ = 10.2/mm at σ_{sat} = 263 MPa; at T = 973 K and t = 1 h, the matrix multi-cracking density increases from φ = 0.21/mm at σ_{cr} = 188 MPa to φ = 8.8/mm at σ_{sat} =263 MPa, and the interface oxidation ratio decreases from ζ/l_d = 26.3 % at σ_{cr} = 188 MPa to ζ/l_d = 13.7 % at σ_{sat} = 263 MPa; and at T = 973 K and t = 3 h, the matrix multi-cracking density increases from φ = 0.15/mm at σ_{cr} = 188 MPa to φ = 7.1/mm at σ_{sat} = 263 MPa, and the interface oxidation ratio decreases from ζ/l_d = 57.2 % at σ_{cr} = 188 MPa to ζ/l_d = = 34.5 % at σ_{sat} = 263 MPa.

At T = 1073 K, the matrix multi-cracking density increases from φ = 0.35/mm at σ_{cr} = 169 MPa to φ = 9.4/mm at σ_{sat} = 236 MPa; at T = 1073 K and t = 1 h, the matrix multi-cracking density increases from φ = 0.2/mm at σ_{cr} = 169 MPa to φ = 7.7/mm at σ_{sat} = 236 MPa, and the interface oxidation ratio decreases from ζ/l_d = 65.7 % at σ_{cr} = 169 MPa to ζ/l_d = 33.2 % at σ_{sat} = 236 MPa; and at T = 1073 K and t = 3 h, the matrix multi-cracking density increases from φ = 0.11/mm at σ_{cr} = 169 MPa to φ = 5.2/mm at σ_{sat} = 236 MPa, and the interface oxidation ratio decreases from ζ/l_d = 1 at σ_{cr} = 169 MPa to ζ/l_d = 68.1 % at σ_{sat} = 236 MPa.

The mini SiC/SiC composite

Zhang et al. [30] investigated the damage evolution of the matrix multi-cracking in the mini-SiC/SiC composite. At room temperature, the matrix multi-cracking evolution starts from the applied stress of σ_{cr} = 135 MPa and approaches saturation at σ_{sat} = 250 MPa; the matrix multi-cracking density increases from φ = 0.4/mm to φ = = 2.4/mm.

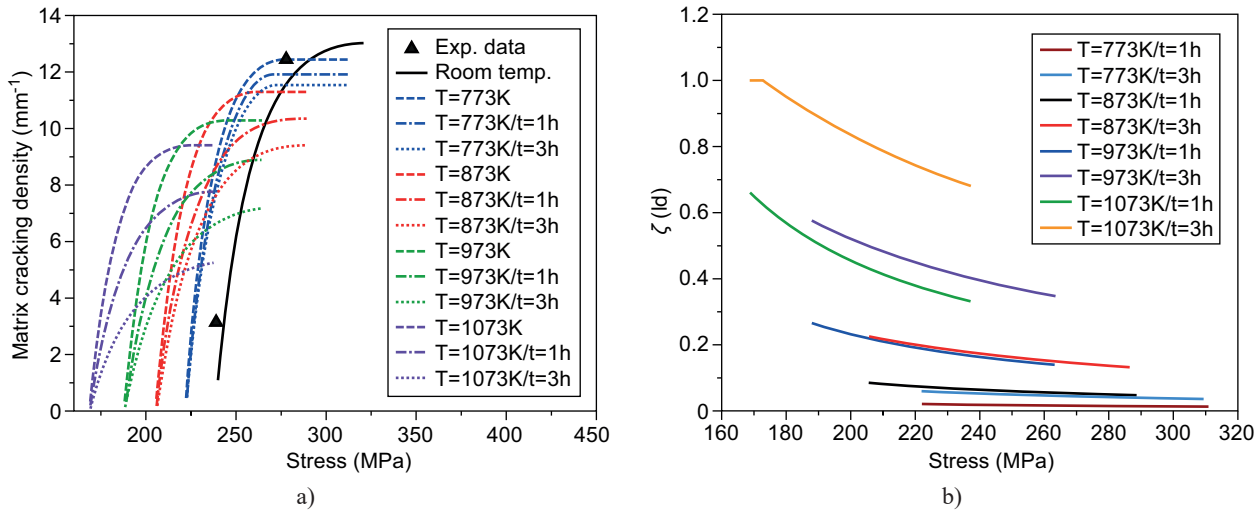

Figure 8. The experimental and theoretical matrix cracking density versus the applied stress curves for the different oxidation temperature and time (a); the interface oxidation ratio versus the applied stress curves for the different oxidation temperature and time of the unidirectional SiC/SiC composite (b).

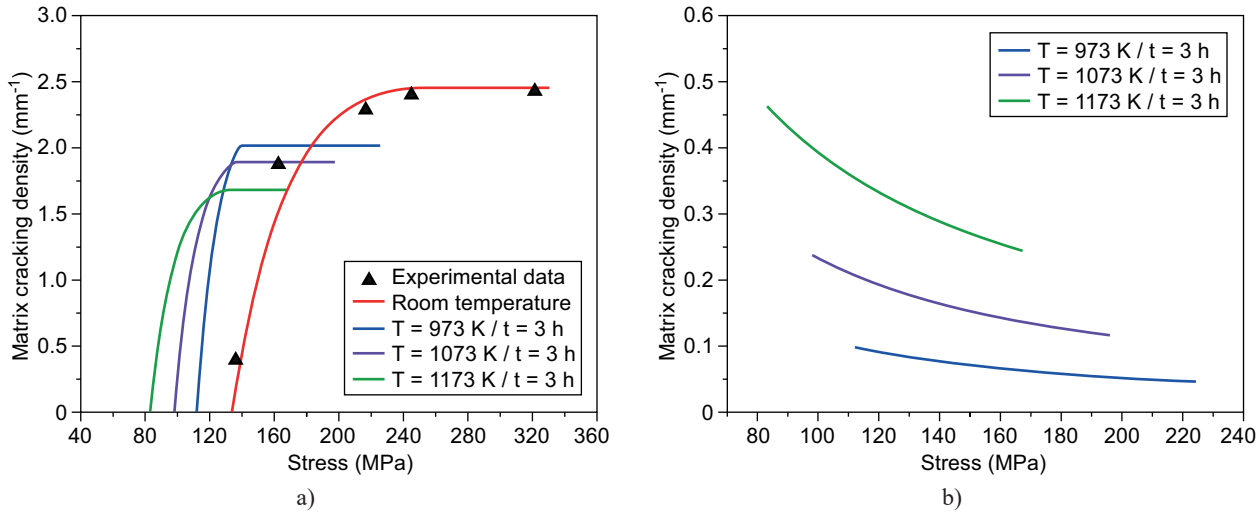

Figure 9. The experimental and theoretical matrix cracking density versus the applied stress curves for the different oxidation temperature and time (a); the interface oxidation ratio versus the applied stress curves for the different oxidation temperature and time of the mini SiC/SiC composite (b).

At T = 973 K and t = 3 h, the matrix multi-cracking density increases from φ = 0.06/mm at σ_{cr} = 112 MPa to φ = 2/mm at σ_{sat} = 140 MPa, and the interface oxidation ratio decreases from ζ/l_d = 9.8 % to ζ/l_d = 4.6 %.

At T = 1073 K and t = 3 h, the matrix multi-cracking density increases from φ = 0.04/mm at σ_{cr} = 98.4 MPa to φ = 1.9/mm at σ_{sat} = 136 MPa, and the interface oxidation ratio decreases from ζ/l_d = 23.7 % to ζ/l_d = 11.6 %.

At T = 1173 K and t = 3 h, the matrix multi-cracking density increases from φ = 0.03/mm at σ_{cr} = 83.4 MPa to φ = 1.7/mm at σ_{sat} = 133 MPa, and the interface oxidation ratio decreases from ζ/l_d = 46.2 % to ζ/l_d = 24.5 %.

CONCLUSIONS

In this paper, the time-dependent matrix multi-cracking of SiC/SiC composite has been investigated considering the fibre/matrix interface oxidation. The effects of the fibre volume fraction, the fibre/matrix interface shear stress, the fibre/matrix interface frictional coefficient, the fibre/matrix interface de-bonded energy and the matrix fracture energy on the matrix multi-cracking density and the fibre/matrix interface oxidation ratio of the SiC/SiC composite have been discussed for the different temperatures and oxidation time. The experimental matrix multi-cracking density and the fibre/matrix interface oxidation ratio for the unidirectional and mini SiC/SiC composite at the different testing temperatures and oxidation time have been predicted.
With an increasing temperature, the first matrix cracking stress of the SiC/SiC composite decreases due to the decreasing of the fibre/matrix interface shear stress in the de-bonded region.

With an increasing of oxidation time at an elevated temperature, the saturation matrix cracking density of the SiC/SiC composite decreases, due to the decreasing of the interface shear stress in the oxidation region.

Acknowledgements

The work reported here is supported by the Fundamental Research Funds for the Central Universities (Grant No. NS2016070).

REFERENCES

1. Christin F. (2002): Design, fabrication, and application of thermostructural composites (TSC) like C/C, C/SiC, and SiC/SiC composites. *Advanced Engineering Materials*, *4*(12), 903-912. doi: 10.1002/adem.200290001
2. Naslain R. (2004): Design, preparation and properties of non-oxide CMCs for application in engines and nuclear reactors: an overview. *Composites Science and Technology*, *64*(2), 155-170. doi: 10.1016/S0266-3538(03)00230-6
3. Zhu D. (2018). *Aerospace ceramic materials: thermal, environmental barrier coatings and SiC/SiC ceramic matrix composites for turbine engine applications*. NASA/TM-2018-219884.
4. Cox B. N., Marshall D. B. (1996): Crack Initiation in Fiber-Reinforced Brittle Laminates. *Journal of the American Ceramic Society*, *79*(5), 1181-1188. doi: 10.1111/j.1151-2916.1996.tb08570.x
5. Sevener K. M., Tracy J. M., Chen Z., Kiser J. D., Daly S. (2017): Crack opening behavior in ceramic matrix composites. *Journal of the American Ceramic Society*, *100*(10), 4734-4747. doi: 10.1111/jace.14976
6. Filipuzzi L., Camus, G., Naslain R., Thebault J. (1994): Oxidation mechanisms and Kinetics of 1D-SiC/c/SiC composite materials: I, an experimental approach. *Journal of the American Ceramic Society*, *77*(2), 459-466. doi: 10.1111/j.1151-2916.1994.tb07015.x
7. Lamouroux F., Naslain R., Jouin J. M. (1994): Kinetics and mechanisms of oxidation of 2D woven C/SiC composites: II, theoretical approach. *Journal of the American ceramic society*, *77*(8), 2058-2068. doi: 10.1111/j.1151-2916.1994.tb07097.x
8. Verrilli M. J., Opila E. J., Calomino A., Kiser J. D. (2004): Effect of Environment on the Stress-Rupture Behavior of a Carbon-Fiber-Reinforced Silicon Carbide Ceramic Matrix Composite. *Journal of the American Ceramic Society*, *87*(8), 1536-1542. doi: 10.1111/j.1551-2916.2004.01536.x
9. Halbig M. C., McGuffin-Cawley J. D., Eckel A. J., Brewer D. N. (2008): Oxidation Kinetics and stress effects for the oxidation of continuous carbon fibers within a microcracked C/SiC ceramic matrix composite. *Journal of the American ceramic society*, *91*(2), 519-526. doi: 10.1111/j.1551-2916.2007.02170.x
10. Li. L. (2017): Modeling matrix cracking of fiber-reinforced ceramic-matrix composites under oxidation environment at elevated temperature. *Theoretical and Applied Fracture Mechanics*, *87*, 110-119. doi: 10.1016/j.tafmec.2016.11.003
11. Smith C. E., Morscher G. N., Xia Z. H. (2008): Monitoring damage accumulation in ceramic matrix composites using electrical resistivity. *Scripta Materialia*, *59*(4), 463-466. doi: 10.1016/j.scriptamat.2008.04.033
12. Simon C., Rebillat F., Herb V., Camus G. (2017): Monitoring damage evolution of SiCf/[SiBC] m composites using electrical resistivity: Crack density-based electromechanical modeling. *Acta Materialia*, *124*, 579-587. doi: 10.1016/j.actamat.2016.11.036
13. Gowayed Y., Ojard G., Santhosh U., Jefferson G. (2015): Modeling of crack density in ceramic matrix composites. *Journal of Composite Materials*, *49*(18), 2285-2294. doi: 10.1177/0021998314545188
14. Parthasarathy T. A., Cox B., Sudre O., Przybyla C., Cinibulk M. K. (2018): Modeling environmentally induced property degradation of SiC/BN/SiC ceramic matrix composites. *Journal of the American Ceramic Society*, *101*(3), 973-997. doi: 10.1111/jace.15325
15. Aveston J., Cooper G.A., Kelly A. (1971). The Properties of Fiber Composites. in: Proceedings of National Physical Laboratory. Guildford, IPC Science and Technology Press. pp. 15–26.
16. Beyerle D. S., Spearing S. M., Zok F. W., Evans A. G. (1992): Damage and failure in unidirectional ceramic-matrix composites. *Journal of the American Ceramic Society*, *75*(10), 2719-2725. doi: 10.1111/j.1151-2916.1992.tb05495.x

17. Holmes J. W., Cho C. (1992): Experimental Observations of Frictional Heating in Fiber-Reinforced Ceramics. *Journal of the American Ceramic Society*, *75*(4), 929-938. doi: 10.1111/j.1151-2916.1992.tb04162.x
18. Kuo W. S., Chou T. W. (1995): Multiple Cracking of Unidirectional and Cross-PlyCeramic Matrix Composites. *Journal of the American Ceramic Society*, *78*(3), 745-755. doi: 10.1111/j.1151-2916.1995.tb08242.x
19. Li L. (2017): Modeling first matrix cracking stress of fiber-reinforced ceramic-matrix composites considering fiber fracture. *Theoretical and Applied Fracture Mechanics*, *92*, 24-32. doi: 10.1016/j.tafmec.2017.05.004
20. Li L. (2017): Synergistic effects of fiber debonding and fracture on matrix cracking in fiber-reinforced ceramic-matrix composites. *Materials Science and Engineering: A*, *682*, 482-490. doi: 10.1016/j.msea.2016.11.077
21. Li L. (2018). *Damage, fracture and fatigue of ceramic-matrix composites*. Springer Nature Singapore Pte Ltd. doi: 10.1007/978-981-13-1783-5
22. Morscher G. N., Singh M., Kiser J. D., Freedman M., Bhatt R. (2007): Modeling stress-dependent matrix cracking and stress–strain behavior in 2D woven SiC fiber reinforced CVI SiC composites. *Composites Science and Technology*, *67*(6), 1009-1017. doi: 10.1016/j.compscitech.2006.06.007
23. Morscher G. N., Gordon N. A. (2017): Acoustic emission and electrical resistance in SiC-based laminate ceramic composites tested under tensile loading. *Journal of the European Ceramic Society*, *37*(13), 3861-3872. doi: 10.1016/j.jeurceramsoc.2017.05.003
24. Racle E., Godin N., Reynaud P., Fantozzi G. (2017): Fatigue lifetime of ceramic matrix composites at intermediate temperature by acoustic emission. *Materials*, *10*(6), 658. doi: 10.3390/ma10060658
25. Gao Y. C., Mai Y. W., Cotterell B. (1988): Fracture of fiber-reinforced materials. *Zeitschrift für angewandte Mathematik und Physik ZAMP*, *39*(4), 550-572. doi: 10.1007/BF00948962
26. Solti J.P., Mall S., Robertson D. D. (1995): Modeling damage in unidirectional ceramic-matrix composites. *Composites Science and Technology*, *54*(1), 55-66. doi: 10.1016/0266-3538(95)00041-0
27. Snead L. L., Nozawa T., Katoh Y., Byun T. S., Kondo S., Petti D. A. (2007): Handbook of SiC properties for fuel performance modeling. *Journal of Nuclear Materials*, *371*(1-3), 329-377. doi: 10.1016/j.jnucmat.2007.05.016
28. Wang R., Li W., Li D., Fang D. (2015): A new temperature dependent fracture strength model for the ZrB_2–SiC composites. *Journal of the European Ceramic Society*, *35*(10), 2957-2962. doi: 10.1016/j.jeurceramsoc.2015.03.025
29. Beyerle D. S., Spearing S. M., Zok F. W., Evans A. G. (1992): Damage and failure in unidirectional ceramic–matrix composites. *Journal of the American Ceramic Society*, *75*(10), 2719-2725. doi: 10.1111/j.1151-2916.1992.tb05495.x
30. Zhang S., Gao X., Chen J., Dong H., Song Y. (2016): Strength model of the matrix element in SiC/SiC composites. *Materials & Design*, *101*, 66-71. doi: 10.1016/j.matdes.2016.03.166